Molecular Biology of the Cell
Vol. 20, 4471–4488, November 1, 2009

Myosin Vc Is a Molecular Motor That Functions in Secretory Granule Trafficking

Damon T. Jacobs,* Roberto Weigert,† Kyle D. Grode,* Julie G. Donaldson,‡ and Richard E. Cheney*

*Department of Cell and Molecular Physiology, School of Medicine, University of North Carolina at Chapel Hill, Chapel Hill, NC 27599; †National Institute of Dental and Craniofacial Research, and ‡Laboratory of Cell Biology, National Heart, Lung, and Blood Institute, National Institutes of Health, Bethesda, MD 20892

Submitted August 22, 2008; Revised August 3, 2009; Accepted August 28, 2009
Monitoring Editor: Thomas F.J. Martin

Class V myosins are actin-based motor proteins that have critical functions in organelle trafficking. Of the three class V myosins expressed in mammals, relatively little is known about Myo5c except that it is abundant in exocrine tissues. Here we use MCF-7 cells to identify the organelles that Myo5c associates with, image the dynamics of Myo5c in living cells, and test the functions of Myo5c. Endogenous Myo5c localizes to two distinct compartments: small puncta and slender tubules. Myo5c often exhibits a highly polarized distribution toward the leading edge in migrating cells and is clearly distinct from the Myo5a or Myo5b compartments. Imaging with GFP-Myo5c reveals that Myo5c puncta move slowly (~30 nm/s) and microtubule independently, whereas tubules move rapidly (~440 nm/s) and microtubule dependently. Myo5c puncta colocalize with secretory granule markers such as chromogranin A and Rab27b, whereas Myo5c tubules are labeled by Rab8a. TIRF imaging indicates that the granules can be triggered to undergo secretion. To test if Myo5c functions in granule trafficking, we used the Myo5c tail as a dominant negative and found that it dramatically perturbs the distribution of granule markers. These results provide the first live-cell imaging of Myo5c and indicate that Myo5c functions in secretory granule trafficking.

INTRODUCTION

Class V myosins are an evolutionarily ancient group of molecular motors that mediate actin-dependent organelle trafficking (Provance and Mercer, 1999; Berg *et al.*, 2001; Trybus, 2008). In the yeast *Saccharomyces cerevisiae*, the class V myosin known as Myo2p localizes to secretory vesicles and functions as a molecular motor that transports these vesicles along actin cables to sites of polarized secretion (Johnston *et al.*, 1991; Pruyne *et al.*, 1998; Karpova *et al.*, 2000). In animal cells, organelles generally undergo long-range movements using microtubule-based motors and the class V myosins appear to function primarily in the actin-rich cell cortex. Class V myosins in animal cells have thus been hypothesized to act as short-range transporters and/or actin-based tethers that function in organelle distribution and exocytosis (Wu *et al.*, 1998; Langford, 2002; Rose *et al.*, 2002; Nascimento *et al.*, 2003; Eichler *et al.*, 2006; Desnos *et al.*, 2007a). Although mammals express three different class V myosins, myosin-Va (Myo5a), myosin-Vb (Myo5b), and myosin-Vc (Myo5c; Rodriguez and Cheney, 2002), little is known about the localization, dynamics, or functions of Myo5c.

Class V myosins have a generally conserved structure that can be divided into a head, neck, and tail (Cheney *et al.*, 1993; Trybus, 2008). The head consists of a myosin motor domain that binds to actin filaments and hydrolyzes ATP to produce force, and the neck consists of six IQ motifs that provide binding sites for up to six calmodulin or calmodulin-like light chains (Espreafico *et al.*, 1992). The tail consists of a largely coiled coil region followed by a globular domain important for organelle binding (Pashkova *et al.*, 2006). Biochemical studies with vertebrate Myo5a indicate that its heavy chains dimerize via their coiled coil regions to form a two-headed molecule that moves processively along actin filaments at rates of 200-1000 nm/s (Cheney *et al.*, 1993; Wu *et al.*, 2006). Mammalian Myo5b also forms dimers, is processive, and can power movement at ~200 nm/s (Watanabe *et al.*, 2006). Although the three class V myosins in mammals are predicted to have similar overall structures, their heavy chains only share 50–60% protein sequence identity, and they have different patterns of expression (Rodriguez and Cheney, 2002).

Myo5a has been the subject of intensive study and is expressed at relatively high levels in neurons and melanocytes, where it is involved in the transport and localization of several different organelles (Desnos *et al.*, 2007a). Myo5a mutations in mouse (*dilute lethal*) and human (Griscelli syndrome) demonstrate that Myo5a functions in melanosome transport/localization and in the localization of smooth endoplasmic reticulum (ER) within dendritic spines (Mercer *et al.*, 1991; Takagishi *et al.*, 1996; Pastural *et al.*, 1997). Myo5a is also expressed in endocrine cells, where it is involved in the localization of endocrine secretory granules (Rose *et al.*, 2002; Rudolf *et al.*, 2003; Varadi *et al.*, 2005). Myo5b is expressed in many different tissues (Zhao *et al.*, 1996), and expressing the Myo5b tail as a dominant negative in HeLa cells leads to the formation of perinuclear puncta that contain Myo5b tail, Rab11a, and transferrin receptor (Lapierre *et al.*, 2001). Ex-

This article was published online ahead of print in *MBC in Press* (http://www.molbiolcell.org/cgi/doi/10.1091/mbc.E08–08–0865) on September 9, 2009.

Address correspondence to: Richard E. Cheney (CheneyR@med.UNC.edu).

pression of the Myo5b tail has been used to show that Myo5b functions in the trafficking of several other important cell surface receptors including the CXCR2 chemokine receptor (Fan *et al.*, 2004), GluR1 glutamate receptor (Lise *et al.*, 2006), and the cystic fibrosis transmembrane receptor (CFTR; Swiatecka-Urban *et al.*, 2007). Together these results indicate that Myo5b functions in exocytic trafficking from a Rab11a-associated recycling compartment.

Myo5c is the third and final member of the class V myosins to be identified in mammals and is expressed most abundantly in exocrine tissues such as pancreas, prostate, and mammary gland (Rodriguez and Cheney, 2002). Expressing the Myo5c tail in HeLa cells leads to the formation of peripheral puncta that contain the Myo5c tail, Rab8a, and transferrin receptor (Rodriguez and Cheney, 2002). This suggests that in HeLa cells, Myo5c associates with a transferrin-recycling compartment that is distinct from the Myo5b/Rab11a recycling endosome. Unfortunately, the localization of endogenous Myo5c in cell lines remains unknown, in part because of relatively low levels of expression in cell lines such as HeLa. In tissues, Myo5c localizes to the actin-rich apical regions of epithelial cells in colon and exocrine pancreas, which led to the suggestion that Myo5c is a class V myosin that functions in exocrine secretory cells (Rodriguez and Cheney, 2002). Consistent with a role in exocrine secretion, Myo5c has been identified in proteomic screens of zymogen granules from pancreas (Chen *et al.*, 2006). Importantly, recent experiments show that Myo5c is present on mature secretory granules in lacrimal gland acinar cells and that expressing the dominant negative Myo5c tail inhibits carbachol-induced secretion (Marchelletta *et al.*, 2008). Although baculovirus-expressed Myo5c constructs can power movement at rates of 24–160 nm/s, Myo5c does not appear to be processive (Watanabe *et al.*, 2007; Takagi *et al.*, 2008). This suggests that several Myo5c molecules would be required to transport a single organelle. The discovery of Myo5c and its association with exocrine secretion raises numerous questions about the basic cell biology of Myo5c. Here we use MCF-7 cells as a cellular model to investigate the localization, dynamics, and functions of this largely uncharacterized motor protein.

MATERIALS AND METHODS

Cloning and Constructs

To generate a full-length Myo5c construct tagged with enhanced green fluorescent protein (GFP-Myo5c, aa 1–1742), an N-terminal 4.0-kb Myo5c fragment was obtained by PCR from a human pancreas cDNA library (Clontech, Palo Alto, CA) using Takara LA polymerase (Takara Bio, Shiga, Japan) and Myo5c primers (5′-tactcgagcatggcggtggccgagctgtac-3′ and 5′-gcggtcgacatcattggcttttccaattgtctt-3′). This fragment was spliced into the existing GFP-Myo5c full tail construct (aa 902-1742 in pEGFP-C2; Rodriguez and Cheney, 2002) using an in-frame XhoI site at the N-terminus and SwaI. GFP-Myo5c HMM (aa 1–1350) and GFP-Myo5c full tail S1539D (aa 1110–1742) were generated by PCR using GFP-Myo5c or GFP-Myo5c full tail as templates, cloned into pTopo2.1, digested with XhoI and BamHI, and inserted into pEGFP-C2. Full-length wild-type rat GFP-Myo5b in pEGFP-C2 was generously provided by Dr. James Goldenring and Joseph Roland of Vanderbilt University (Lapierre *et al.*, 2001). GFP-Myo5b full tail (aa 912-1846) was generated by PCR from GFP-Myo5b using specific primer sequences (5′-ataataagcttcgaggcccgttctgca-3′ and 5′gcgataggatccycagacttcattgaggaa-3′), cloned into pTopo2.1, digested with XhoI and BamHI, and inserted into pEGFP-C2. Human brain GFP-Myo5a full tail in pEGFP-C1 (aa 911-1855; "pEGFP-MyoVaLT"), neuropeptide Y-monomeric red fluorescent protein (NPY-mRFP), and NPY-GFP were generously provided by Drs. Francois Darchen, Clare Desnos, and Jean-Pierre Henry (Institute de Biologie Physico-Chimique, Paris; Desnos *et al.*, 2007b). Chromogranin A-GFP (Taupenot *et al.*, 2002) was generously provided by Dr. Ann Erickson (UNC Chapel Hill). The mCherry color cassette cDNA sequence was obtained by PCR from an mCherry-α-tubulin plasmid (generously provided by Dr. Roger Tsien, HHMI/UCSD) using primer sequences (5′-gctaccggtcgccaccatggtgagcaag-3′ and 5′-gctcgagatcttgagtccggacttgtac-3′). mCherry-5.2 (empty vector), mCherry-Myo5c, mCherry-Myo5c full tail, and mCherry-Myo5b were constructed by inserting mCherry in place of GFP in pEGFP-C2 or the relevant GFP-myosin using the N-terminal AgeI restriction site and the XhoI restriction site within the multiple cloning site. PCR reactions were performed using PFU Ultra HF DNA polymerase (Stratagene, La Jolla, CA), and new constructs were verified by restriction enzyme digestion and sequencing.

Antibodies and Reagents

Affinity-purified rabbit anti-Myo5a (clone 32a), chicken anti-Myo5b (no. 1961), and rabbit anti-Myo5c (no. 200) were described previously (Rodriguez and Cheney, 2002). Other antibodies used in this study were monoclonal anti-lipase (Cortex Biochem, San Leandro, CA), monoclonal anti-transferrin receptor C2063 (Sigma, St. Louis, MO), monoclonal anti-EEA1 and monoclonal anti-GM130 (BD Biosciences, San Jose, CA), monoclonal anti-CD63 and monoclonal anti-LAMP1 H4A3 (Developmental Studies Hybridoma Bank, University of Iowa, Iowa City, IA), monoclonal anti-Golgin97 CDF4 and monoclonal anti-protein disulfide isomerase (PDI) S34200 (Invitrogen, Carlsbad, CA), sheep anti-TGN46 (ABD-Serotec), monoclonal anti-HSC70 13D3 and monoclonal anti-mannose-6-phosphate receptor 2G11 (Affinity BioReagents, Golden, CO), rabbit anti-Exo70 (Yeaman *et al.*, 2004; generously provided by Dr. Patrick Brennwald, UNC Chapel Hill), rabbit anti-Rab3d (Evans *et al.*, 2004; generously provided by Dr. C. William Davis, UNC Chapel Hill), rabbit anti-Rab8a (generously provided by Dr. Johan Peranen, University of Helsinki), rabbit anti-Rab11a (Invitrogen), rabbit anti-Rab27b (Strategic Diagnostics, Newark, DE), and monoclonal anti-GFP JL-8 (Clontech). Goat secondary antibodies (Alexa-488 and Alexa-568) specific for IgG from mouse, rabbit, or sheep were obtained from Invitrogen.

Cell Culture

MCF-7 cells were grown in complete media consisting of minimal essential medium (MEM; Invitrogen) supplemented with 10% fetal bovine serum (Sigma), 1% penicillin/streptomycin, 10 μg/ml insulin, 1% nonessential amino acids, and 1% sodium pyruvate. HeLa cells were grown in MEM supplemented with 10% fetal bovine serum and 1% penicillin/streptomycin. All cells were cultured at 37°C with 5% CO_2.

Transient Transfections

For transient expression experiments, MCF-7 cells were plated onto no. 1.5 glass coverslips (12 mm round or 22 mm square) for 12–24 h before transfection. Transient transfection of MCF-7 cells was achieved using PolyFect transfection reagent (Qiagen, Chatsworth, CA) according to manufacturer's recommendations for adherent HeLa cells in a six-well plate. Myosin constructs were generally imaged 8–24 h after transfection. Chromogranin and NPY constructs were imaged 24–48 h after transfection to get clear labeling of secretory granules rather than ER and Golgi.

Generation of MCF-7 (DJ32) Cells That Stably Express GFP-Myo5c

MCF-7 cells were transfected with full-length GFP-Myo5c as described above and then subjected to selection with 1.25 μg/ml Geneticin (Gibco Life Technologies, Rockville, MD). Isolated clones were maintained under selection and were screened for GFP-Myo5c expression using fluorescence microscopy and immunoblotting with antibodies to Myo5c and GFP.

Immunoblotting

Cells were trypsinized with 0.25% trypsin with EDTA and counted to allow for equal loading based on cell number. Cells were collected by centrifugation at 1000 × *g* in 1.5-ml tubes, resuspended in phosphate-buffered saline (PBS) with 5× Complete Protease Inhibitor Cocktail (Roche, Indianapolis, IN), mixed with hot 5× SDS sample buffer, heated for 10 min at 90°C, flash-frozen in liquid nitrogen, and stored at −80°C until use. SDS-PAGE on 4–12% gels was followed by transfer at 4°C for 400 V-hours in an LE-22 transfer chamber (Hoefer Scientific Instruments, San Francisco, CA). Blots were stained with Ponceau S to confirm transfer and equal loading. Blots were then blocked for 1 h with 5% dried milk in Tris-buffered saline plus 0.05% Tween 20 (TBST) and incubated 1–4 h at room temperature with 1 μg/ml primary antibody. Blots were then washed three times with TBST and incubated with HRP-conjugated donkey anti-rabbit secondary antibody (Jackson ImmunoResearch Laboratories, West Grove, PA) diluted 1:15,000 in TBST for 1 h followed by three 10-min washes in TBST. Blots were developed using chemiluminescence and scanned using an Epson 1680 scanner (Long Beach, CA) in 16-bit black-and-white mode and then analyzed using Photoshop 6.0 (Adobe Systems, San Jose, CA) and Metamorph software (Universal Imaging, West Chester, PA). For quantification, images were inverted, background was subtracted, and then the Metamorph "Region Measurements" function was used to determine the integrated intensity of each band.

Immunofluorescence

Cells were plated onto 12-mm round glass coverslips and cultured overnight or longer. Cells were fixed using 2–4% paraformaldehyde in PBS for 10 min at 37°C, followed by three washes of 10 min each in PBS. For methanol

fixation, cells were incubated in 95% methanol with 5 mM EGTA at −20°C for 20 min, extracted with 100% acetone for 2 min at room temperature, and then washed in PBS three times for 10 min each. Otherwise cells were permeabilized using 0.2–0.5% Triton X-100 in PBS for 10 min at room temperature and washed in PBS three times for 10 min each. Cells were incubated in blocking solution (5% goat serum in PBS, pH 7.2, [G9023; Sigma] or 2% BSA [A4503; Sigma] in PBS) for 1 h. Primary antibodies at ~1 μg/ml in blocking solution were incubated for 1–12 h at room temperature, followed by three washes in PBS +0.1% goat serum. Incubations with 1 μg/ml secondary antibodies performed similarly except that incubations were for ~3 h and were followed by three washes in PBS. Staining with 13 nM Alexa-568 phalloidin (Invitrogen) was performed either during incubation with secondary antibody or in a subsequent incubation in PBS. Coverslips were mounted using GelMount mounting media (Biomeda, Foster City, CA).

Imaging

In live-cell imaging experiments, MCF-7 cells were equilibrated in imaging media (Opti-MEM I, Invitrogen) for 0.5–2 h before imaging at 34–37°C in an enclosed imaging chamber (Rose chamber). Drugs were perfused by gravity at ~2.0 ml/min. Live-cell imaging was performed on a Nikon TE2000U inverted microscope (Melville, NY) with a 60× (1.45 NA) objective equipped for differential interference contrast (DIC), wide-field epifluorescence, and objective-based total internal reflection fluorescence (TIRF) with a Nikon TIRF II illuminator. TIRF imaging for quantification of GFP puncta was performed using the same equipment, conditions and the settings we recently reported for live-cell single-molecule experiments (Kerber *et al.*, 2009). Two-color TIRF experiments were performed using the 488-nm line of a 300-mW Argon gas laser and the 568-nm line from a 120-mW mixed gas Argon/Krypton laser. GFP and Alexa 488 were imaged with a Chroma 41001 GFP filter set (Brattleboro, VT), and red fluors were imaged with a 41002c TRITC set or a 41004 Texas Red filter set. For dual wavelength TIRF illumination, a Chroma 76653 dual pass dichroic (Z488/568 RDC) was used with a green band-pass (530/35 nm) or a red band-pass (630/60 nm) emission filter in a motorized filter wheel under the control of Metamorph software. For dual TIRF and wide-field imaging, a 60/40 mirror was placed in the illumination path. Confocal images were obtained in 12-bit mode on a Zeiss LSM 510 (Thornwood, NY) using a 63× (1.4 NA) objective with the pinhole generally set to obtain a 1-μm optical section. Confocal illumination was provided by a 30-mW Argon gas laser and a 1-mW HeNe mixed gas laser.

Image Analysis

Manual measurements of puncta diameter were performed by identifying all well-resolved puncta extending across three or more pixels (107 nm/pixel) and then measuring the apparent puncta diameter. For manual measurements of velocity, individual puncta or tubules were tracked frame-by-frame using the "Track Points" function in Metamorph. For tubules, only the tips of tubules that were clearly detectable in wide-field epifluorescence were tracked.

Automated particle tracking and velocity measurements were performed with DiaTrack 3.03 Pro software (Semasopht, Renens, Switzerland; Vallotton and Small, 2009). Particles were identified using the "Local Maxima" algorithm, a ~0.5 filter setting, and "Trash Dim" was adjusted to eliminate background particles. "Trash Bright" was used at the default setting, and "Trash Blurred" was adjusted to eliminate out of focus particles. Tracking was carried out in the "High Precision" mode and results from the "Track-based Distributions" menu were exported to Excel (Microsoft, Redmond, WA) for analysis. For every particle that could be tracked for five or more consecutive frames, the average velocity along the track was calculated.

Colocalization analysis was performed using confocal images that were background-subtracted based on the average intensity of a 100 × 100-pixel region adjacent to the cell being evaluated. A 90% lower limit threshold was then applied to the images, and the Metamorph "Find Spots" function was used to define individual regions corresponding to puncta in the "green" color channel. The regions identified in this way were then overlaid onto the image from the red channel. Each green region was then manually scored as either "colocalized" or "not colocalized" with signal in the red channel. Linescans of the fluorescence intensity across single secretory granules were generated using the Metamorph "Measure Linescan" function and a line width of 1 pixel. Image registration was adjusted using 0.1-μm Tetraspeck microspheres (Invitrogen) and the color align function in Metamorph. Numerical values are reported as mean ± SD, and statistical significance was determined using a two-tailed Student's *t* test.

Scoring of Granule Aggregation Induced by the Myo5c Tail

MCF-7 cells transfected with the indicated constructs were imaged under identical acquisition settings that allowed clear detection of individual granules in control cells. The images were then background-corrected by subtracting the average intensity in a 100 × 100-pixel region outside the cell and thresholded by the same value for all images to define regions corresponding to granules. The area, effective diameter, and integrated intensity were then determined for every thresholded region whose effective diameter was greater than 0.2 μm. For each cell, the percentage of the total granule fluorescence arising from granules with apparent diameters greater than 1 μm was then calculated by dividing the summed fluorescence intensity of all granules with diameters greater than 1 μm by the summed fluorescence intensity of all granules with diameters greater than 0.2 μm. This value was calculated for 3–14 cells for each condition in each experiment. Note that in this assay, which was designed to measure the fluorescence of all the granules in a cell, granules that are too close together to be individually resolved are thresholded as a single larger region.

Single-Granule Fluorescence Recovery after Photobleaching

Experiments were performed using a Zeiss LSM510 with the zoom set to 6× (0.05 μm/pixel) and using the "Edit Bleach/Define Regions" menu to bleach selected granules or control regions with 1.5-μm-diameter spots using the 488-nm line for GFP and the 543-nm line for mRFP at 100% power with 100 iterations each. The integrated fluorescence intensity of each granule was tracked through time using a moving 1.5-μm diameter spot and Metamorph software. The intensity of each spot was corrected for background fluorescence by subtracting the background measured from an adjacent region of cytoplasm lacking secretory granules for each time point. To correct for the gradual bleaching due to repeated imaging, a correction factor for each time point (and each color channel) in a given image series was generated by determining the average bleach rate for three nonbleached granules. The integrated intensity at each time point for each bleached granule was then multiplied by the relevant correction factor. The intensity values for each granule were then normalized based on the granule's average prebleach intensity.

RESULTS

Myo5c Is Expressed in Exocrine Tissues and MCF-7 Cells

To identify the organelles that Myo5c associates with, we first sought to identify a cell line that would allow us to determine the localization of endogenous Myo5c. We thus screened rat tissues using immunoblotting and immunofluorescence to identify cell types that express high levels of Myo5c (Supplemental Figure S1). Consistent with previous results (Rodriguez and Cheney, 2002; Chen *et al.*, 2006), we detected high levels of Myo5c expression in exocrine tissues such as pancreas and prostate. Immunofluorescence showed clear Myo5c staining in the exocrine pancreas, and counterstaining with anti-lipase revealed that Myo5c is largely localized to acinar cells, the chief secretory cells of the exocrine pancreas. A similar pattern of localization was observed in the parotid and prostate glands, where the brightest Myo5c staining was found near the actin-rich region surrounding the secretory lumen. Together these results suggested that Myo5c would be most easily detected in cells derived from exocrine tissues. We thus tested MCF-7 cells, a cell line derived from a human mammary gland adenocarcinoma and found by blotting and densitometry that that they express ~100-fold more Myo5c per cell than HeLa cells (Figure 1A). These results suggested that MCF-7 cells would provide a useful model system that is compatible with high-resolution imaging to investigate the fundamental cell biology of Myo5c.

Endogenous Myo5c Localizes to Puncta and Tubules

Because the localization of Myo5c in cell lines was unknown, we performed immunofluorescence experiments in MCF-7 cells using a previously characterized affinity-purified antibody against Myo5c (Rodriguez and Cheney, 2002). These experiments revealed that endogenous Myo5c localized to small puncta in virtually all MCF-7 cells (Figure 1). There were tens to hundreds of puncta per MCF-7 cell. The apparent diameters of the endogenous Myo5c puncta ranged from 0.3 to 1.1 μm, and the mean was 534 ± 138 nm (537 puncta from eight cells). Puncta were present in the perinuclear region, the cell periphery, and the ventral surface of the cell (Figure 1, C and D). At high magnification, individual

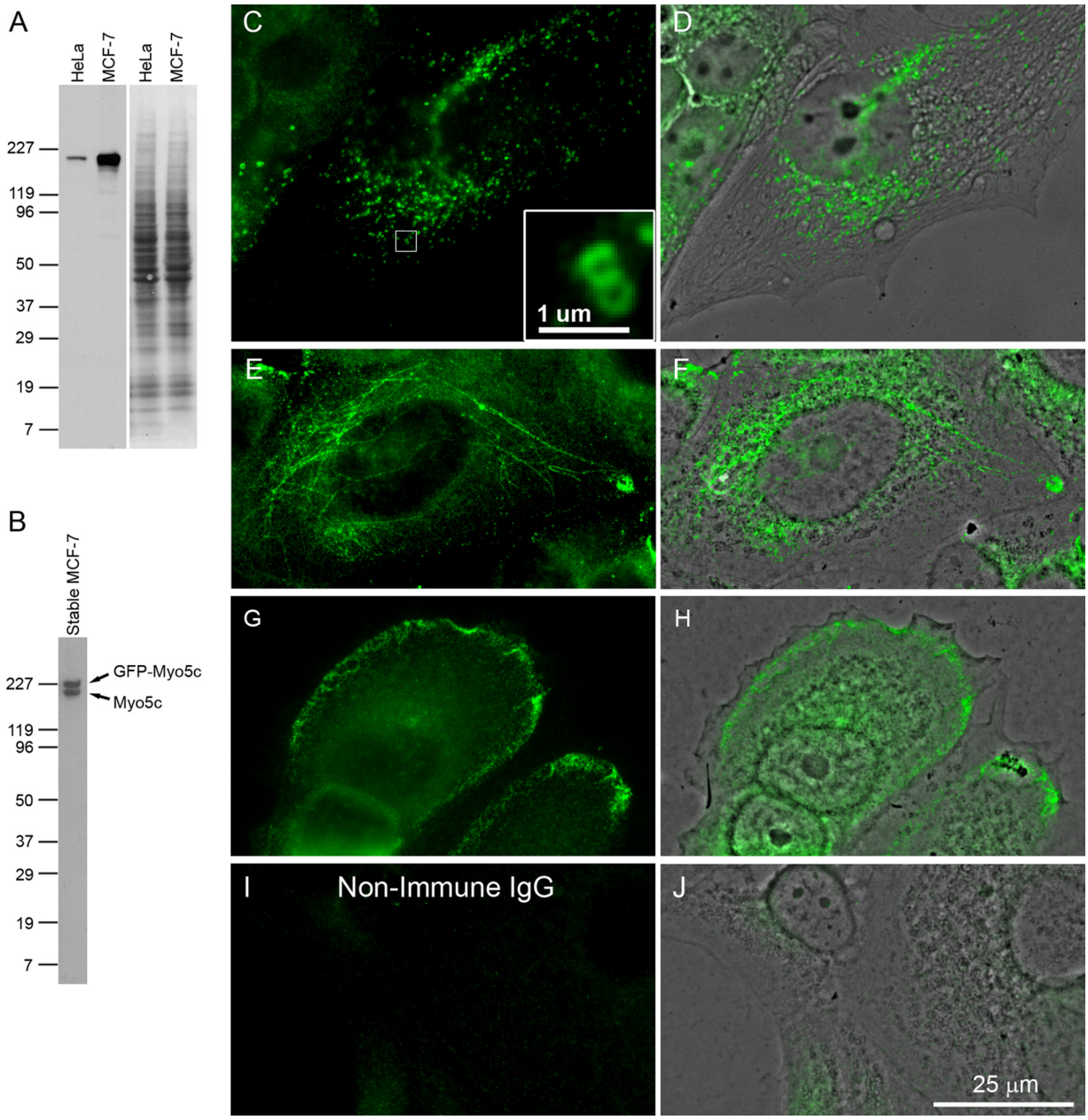

Figure 1. Endogenous Myo5c localizes to small puncta and slender tubules. (A) Immunoblot showing that MCF-7 cells express relatively high levels of Myo5c. SDS lysates of equal numbers of MCF-7 or HeLa cells were run on 4–20% SDS-PAGE gels and transferred to nitrocellulose, stained with Ponceau S (right) to confirm equal protein loading, and then immunoblotted with anti-Myo5c. (B) A similar immunoblot of MCF-7 cells that stably express GFP-Myo5c to illustrate the relative expression levels of GFP-Myo5c (top band) and endogenous Myo5c (bottom band). (C–H) Immunofluorescence images of MCF-7 cells stained with anti-Myo5c. (C and D) Endogenous Myo5c localizes to puncta that are distributed in the perinuclear region, the cell periphery, and the ventral surface. (C, inset) Higher magnification of boxed region showing that individual Myo5c puncta are often ring-like with a hollow center. (E and F) In some cells, endogenous Myo5c also localizes on slender tubules. (G and H) In spreading or migrating cells, Myo5c frequently exhibits a strikingly polarized localization toward the leading edge. Comparison of the fluorescence and phase-contrast images shows that the Myo5c staining does not extend all the way to the leading edge and is instead found in the transition zone behind the lamellipodium. (I and J) MCF-7 cells stained with control antibody shows little labeling. Left panels, representative wide-field fluorescence images alone; right panels, the fluorescence images overlaid with the corresponding phase-contrast images.

puncta of endogenous Myo5c often had a ring-like appearance, as would be expected if Myo5c was present on the cytoplasmic surface of a vesicle or granule (Figure 1C, inset).

In addition to puncta, endogenous Myo5c also localized to slender tubules. These tubules often spanned tens of micrometers, and their morphology suggested that they were membranous (Figure 1, E and F). Myo5c-labeled tubules were detected in ~5–10% of nonconfluent cells and 25% of confluent cells. Puncta of Myo5c were often observed at different points along Myo5c-labeled tubules. In methanol-fixed cells, Myo5c exhibited a similar pattern of localization on puncta, and tubules and the Myo5c-labeled tubules ex-

hibited only occasional sites of overlap with microtubules (not shown). Control antibodies showed only a diffuse background staining (Figure 1, I and J).

In MCF-7 cells that were spreading or migrating, Myo5c puncta were often strikingly polarized toward the leading edge. Comparison of the fluorescence and phase contrast images indicates that the Myo5c puncta were excluded from the leading edge proper and instead localized to the transition zone near the lamellipodium (Figure 1, G and H). The transition zone is located at the interface between the microtubule-rich central region of the cell and the actin-rich periphery and is a region of active exocytosis and endocytosis that contains many membranous organelles (Bergmann *et al.*, 1983; Yvon and Wadsworth, 2000). The highly polarized localization of Myo5c puncta to the transition zone suggests that Myo5c may be associated with trafficking pathways involved in directed insertion near the leading edge (Hopkins *et al.*, 1994; Schmoranzer *et al.*, 2003).

Dynamics of Myo5c in Living Cells

To investigate the dynamics of Myo5c in living cells, we generated a full-length GFP-Myo5c construct with GFP fused to the N-terminus of human Myo5c (see Supplemental Figure S2 for a diagram of all the myosin-V constructs used here). N-terminally tagged myosins have been reported to retain their motor and cargo-binding activities (Moores *et al.*, 1996; Zhang *et al.*, 2004) and have been widely used to image myosin dynamics (Moores *et al.*, 1996; Berg and Cheney, 2002; Belyantseva *et al.*, 2005). When GFP-Myo5c was transiently expressed in MCF-7 cells, it exhibited a pattern of localization very similar to that of endogenous Myo5c. Like endogenous Myo5c, GFP-Myo5c localized to small puncta in all MCF-7 cells and to slender tubules in a subset of MCF-7 cells. Furthermore, in spreading or migrating cells, GFP-Myo5c often exhibited a polarized distribution to the transition zone near the leading edge (Figures 2 and 3).

In addition to transiently transfecting MCF-7 cells with GFP-Myo5c, we also generated an MCF-7 cell line that stably expresses GFP-Myo5c. As expected, immunoblots of the stable cell line revealed expression of a single additional band that was ~28 kDa larger than endogenous Myo5c (Figure 1B). Densitometry of these blots indicates that the stable line expresses GFP-Myo5c at ~1.3 times the level of endogenous Myo5c. The stably expressed GFP-Myo5c yielded the same pattern of localization to puncta, slender tubules, and the transition zone that was observed with endogenous Myo5c (Figures 3 and 4). Together these results indicate that GFP-tagged Myo5c accurately recapitulates the localization of endogenous Myo5c.

Because nothing was known about the dynamics of Myo5c in living cells, we performed live-cell imaging with GFP-Myo5c and found that the Myo5c puncta continuously undergo slow movements that appear randomly directed (Figure 2 and Movie 1). Although puncta of GFP-Myo5c could be observed by either wide-field or TIRF microscopy, TIRF yielded particularly clear images of Myo5c puncta. Because TIRF illumination only excites fluorophores within ~200 nm of coverslip surface, many of the Myo5c puncta are in extremely close proximity to the plasma membrane. Most Myo5c puncta visible by TIRF could be tracked for several minutes, and some remained within the TIRF field for the entire duration of a 38+-min time lapse (Figure 2B). This indicates that Myo5c-labeled puncta are relatively long-lived structures under resting conditions. Manual tracking of the Myo5c puncta yielded an average velocity of 30 ± 29 nm/s (Figure 2E). Addition of 5 μM nocodazole, a microtubule-depolymerizing agent, did not obviously perturb the distribution or velocity (30 ± 35 nm/s) of the Myo5c puncta (Figure 2, E and F; Movie 2). When the image sequences from these experiments were analyzed by automated particle tracking instead of manual tracking, we obtained very similar velocity values (32 ± 18 nm/s from 833 pre-nocodazole tracks and 30 ± 15 nm/s from 741 post-nocodazole tracks).

Live-cell imaging of the GFP-Myo5c–labeled tubules revealed that they are highly dynamic and move much faster than the puncta. Myo5c-labeled tubules extended in a rapid and directed manner over tens of micrometers at rates of ~200–1100 nm/s (Figure 2G and Movie 2). Most tubules appeared to extend toward the cell periphery. Addition of 5 μM nocodazole led to a dramatic loss of the Myo5c tubules and an apparent collapse toward the cell center (see Movie 2). The rapid and directed movements of these tubules, as well as their morphology and sensitivity to nocodazole, indicate that Myo5c associates with a class of membranous tubules that undergo long-range transport along microtubules.

The Localization of Myo5c Is Distinct from that of Myo5a or Myo5b

We next asked if Myo5c associates with different compartments than Myo5a or Myo5b. We thus immunostained cells that stably express GFP-Myo5c with antibodies to Myo5a (Figure 3, A–C). Endogenous Myo5a in MCF-7 cells localized to bright puncta distributed throughout the cell in a pattern similar to that seen in HeLa cells (Rodriguez and Cheney, 2002). Importantly, GFP-Myo5c showed little or no colocalization with Myo5a, indicating that these two myosins associate with different organelles (Figure 3, A–C). Immunostaining with a rabbit nonimmune IgG control showed that the Myo5a antibody staining is specific (Figure 3, D–F), and immunoblotting showed that MCF-7 cells express detectable levels of all three class V myosins (Figure 3J).

We next tested if the localization and dynamics of Myo5c are distinct from those of Myo5b. Although dominant negative experiments have implicated both of these myosins in transferrin receptor recycling (Lapierre *et al.*, 2001; Rodriguez and Cheney, 2002), the distributions of the two myosins have never been directly compared. Furthermore, the dynamics of two different class V myosins have never been visualized simultaneously. We thus performed live-cell imaging experiments on MCF-7 cells cotransfected with a full-length mCherry-Myo5c construct and a previously characterized full-length GFP-Myo5b construct (Lapierre *et al.*, 2001). The mCherry-tagged Myo5c exhibited the same patterns of localization and dynamics we had observed for endogenous Myo5c and GFP-Myo5c (Figure 3, G–I, and Movie 3). Importantly, the mCherry-Myo5c showed little overlap with GFP-Myo5b. The GFP-Myo5b did localize to numerous puncta, and these appeared to be slightly smaller and faster than the Myo5c puncta.

To address this issue more quantitatively, we used wide-field fluorescence microscopy to image cells transiently transfected with either GFP-Myo5b or GFP-Myo5c and measured the diameters and velocities of the puncta. The average diameter of the Myo5b puncta (406 ± 69 nm; 229 puncta from seven cells) was indeed smaller than the average diameter of the GFP-Myo5c puncta (567 ± 114 nm; 459 puncta from five cells; significant at $p < 0.0001$). Using automated particle tracking, we determined that the GFP-Myo5b puncta moved with an average velocity of 62 ± 42 nm/s (4339 tracks from five cells). This is approximately twice the average velocity of 28 ± 16 nm/s obtained in parallel experiments with GFP-Myo5c puncta (1132 tracks from seven

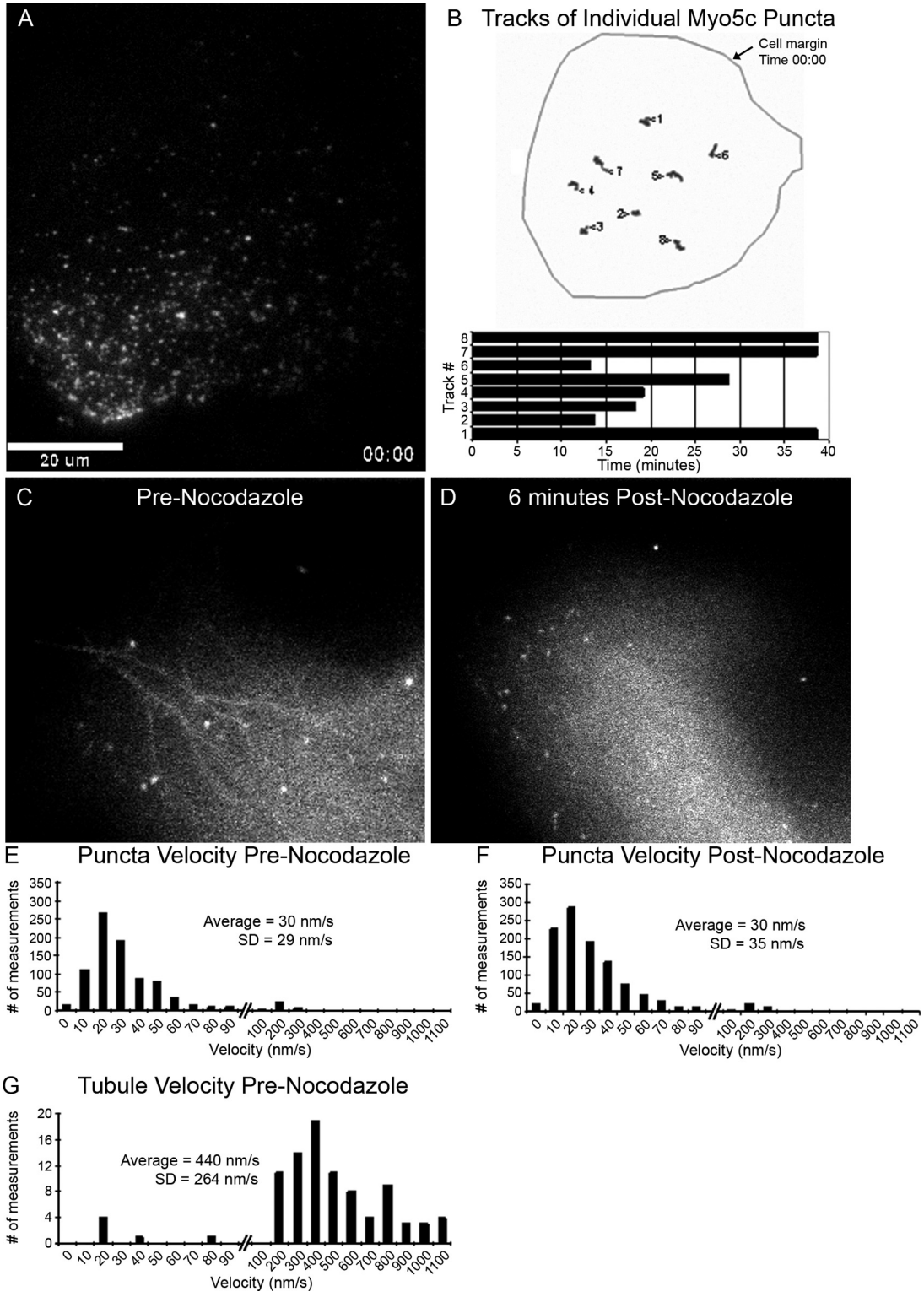

Figure 2. Dynamics of GFP-Myo5c–associated puncta and tubules. (A) TIRF image from a time-lapse experiment showing the localization of GFP-Myo5c to numerous small puncta visible on the ventral surface of an MCF-7 cell. (B) Tracks of selected Myo5c puncta from the cell in A that were visible at the start of the timelapse. The starting positions of the puncta are indicated by the numbered arrowheads and the histogram shows the time during which each puncta remained visible within the TIRF field. Note that the Myo5c puncta move in a slow and apparently random manner and are relatively long lived (see also Movie 1). (C) Wide-field image from a timelapse experiment showing localization of GFP-Myo5c to small puncta and slender tubules in an MCF-7 cell. (D) Wide-field image of the same cell in C 6 min after treatment with 5 μM nocodazole. Note that nocodazole leads to the disappearance of the Myo5c tubules, but not the Myo5c puncta (see also Movie 2). (E) Histogram of the velocities of individual Myo5c puncta before addition of nocodazole (854 measurements). (F) Histogram of the velocities of individual Myo5c puncta after addition of nocodazole (1097 measurements). Myo5c puncta moved slowly before adding

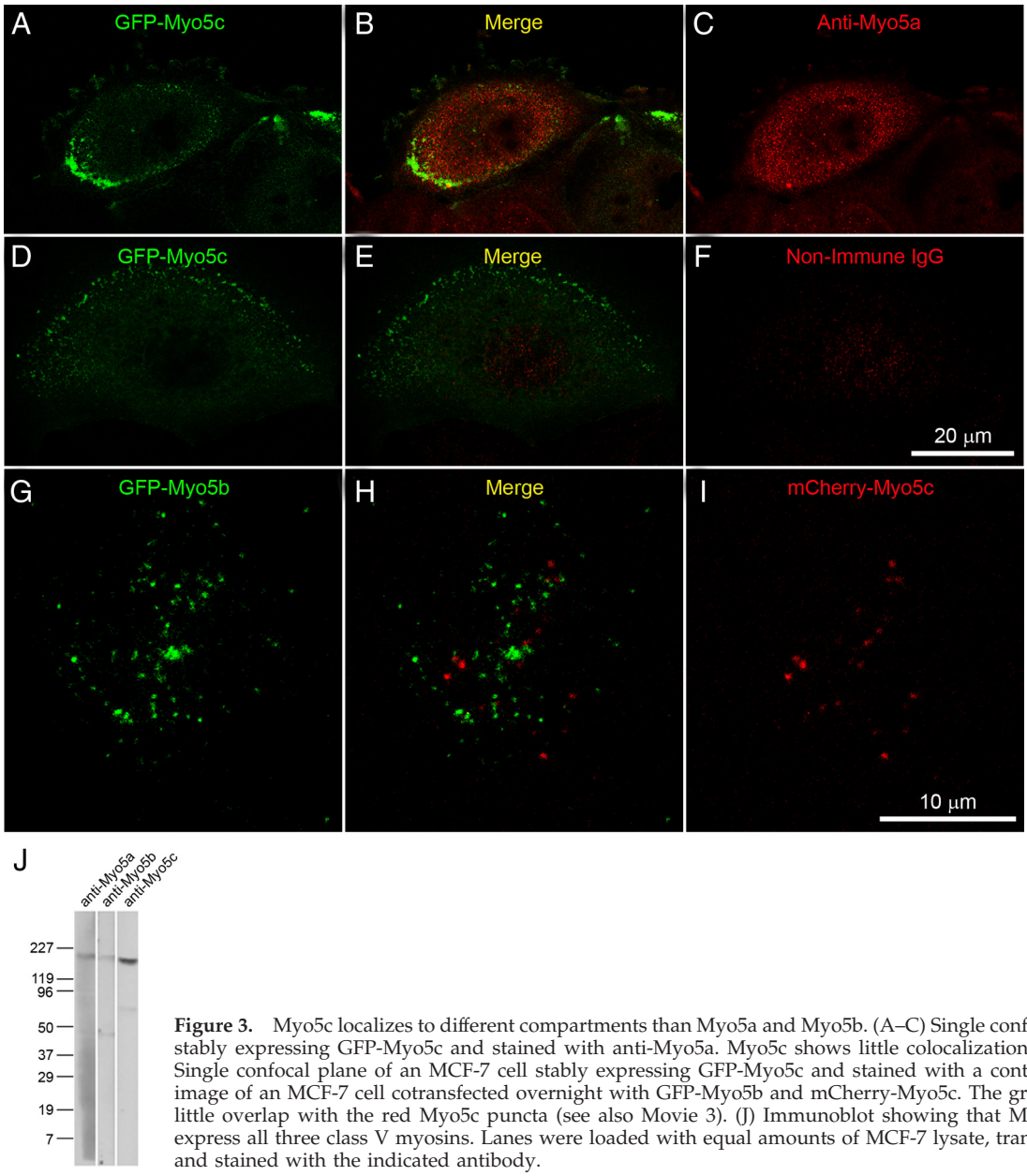

Figure 3. Myo5c localizes to different compartments than Myo5a and Myo5b. (A–C) Single confocal plane of MCF-7 cells stably expressing GFP-Myo5c and stained with anti-Myo5a. Myo5c shows little colocalization with anti-Myo5a. (D–F) Single confocal plane of an MCF-7 cell stably expressing GFP-Myo5c and stained with a control antibody. (G–I) TIRF image of an MCF-7 cell cotransfected overnight with GFP-Myo5b and mCherry-Myo5c. The green Myo5b puncta show little overlap with the red Myo5c puncta (see also Movie 3). (J) Immunoblot showing that MCF-7 cells endogenously express all three class V myosins. Lanes were loaded with equal amounts of MCF-7 lysate, transferred to nitrocellulose, and stained with the indicated antibody.

cells; significant at $p < 0.0001$). Although Movie 3 shows that Myo5b puncta do occasionally appear to transiently contact or overlap with Myo5c puncta, the experiments here clearly demonstrate that Myo5c and Myo5b localize to largely distinct compartments.

Figure 2 (cont). nocodazole and continued to move slowly in the presence of nocodazole (data from two experiments with three cells). (G) Histogram showing the rapid extension rates of Myo5c tubules before addition of nocodazole (92 measurements). Note that the histograms use 10-nm/s bins for velocities below 100 nm/s and 100-nm/s bins for velocities above 100 nm/s. Because the Myo5c tubules disappeared after addition of nocodazole, there are no postnocodazole measurements of tubule velocity. Cells were transfected with GFP-Myo5c and incubated overnight before imaging.

With What Organelles Does Myo5c Associate?

To identify the specific organelle(s) that Myo5c associates with, we performed double-labeling experiments with markers for different membrane compartments (Figure 4). Confocal images showed little or no colocalization of endogenous Myo5c with markers for early endosomes (EEA1), the transferrin recycling pathway (transferrin receptor), multivesicular bodies (CD63), or the ER (protein disulfide isomerase [PDI]; Figure 4, A–I). Myo5c also showed little colocalization with a marker for the *trans*-Golgi network (TGN46), although it should be noted that faint Myo5c labeling was sometimes detected near the TGN (Figure 4, J and K). We also observed little or no colocalization with markers for the Golgi apparatus (Golgin 97), late endosomes (mannose-6-phosphate receptor), or lysosomes (LAMP-1; not shown). Interestingly, antibodies to Exo70 did partially colocalize with Myo5c on slender tubules

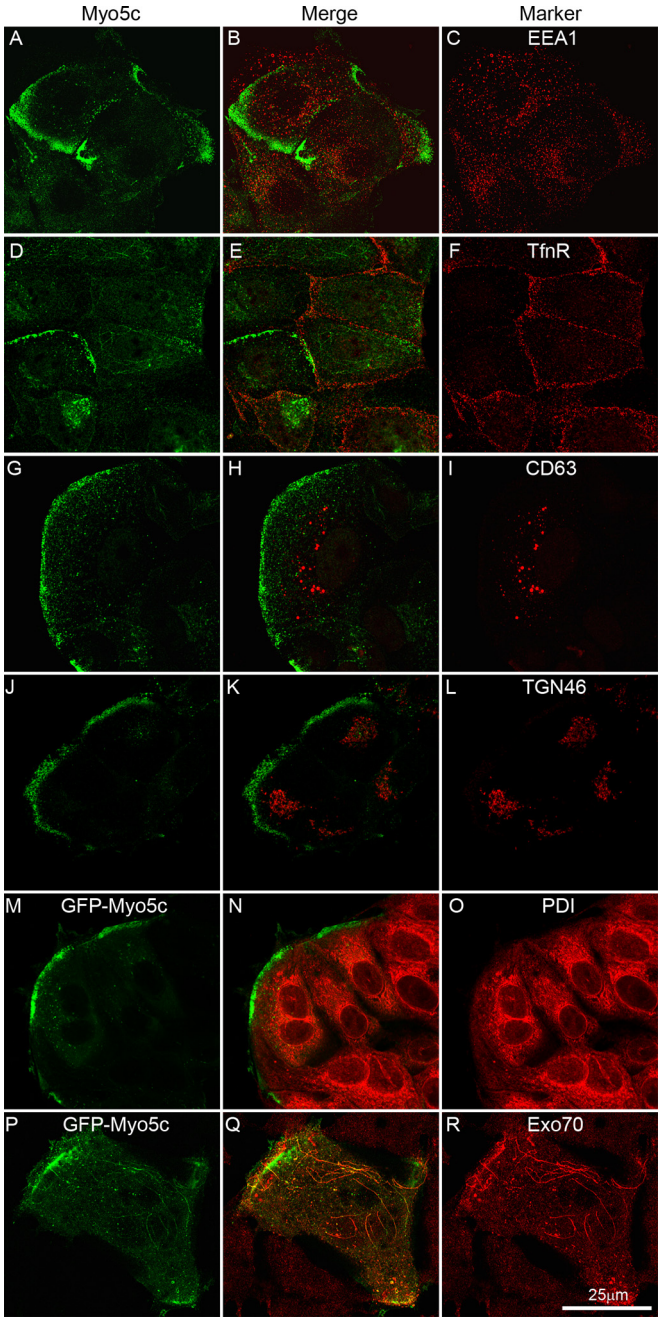

Figure 4. Distribution of Myo5c relative to selected membrane compartments. Endogenous Myo5c (A, D, G, and J) and stably expressed GFP-Myo5c (M and P) localize to puncta and tubules in MCF-7 cells. The middle panels are merged images of Myo5c and compartment markers (B, E, H, K, N, and Q). Myo5c showed little or no overlap with known markers of endocytic compartments such as anti-EEA1 (C) or anti-transferrin receptor (F). Myo5c also showed little or no overlap with anti-CD63, a marker for late endosomes and multivesicular bodies (I). Anti-TGN46 (L), a marker of the *trans*-Golgi network, and protein disulfide isomerase (PDI; O), a marker of the ER, also showed little overlap with GFP-Myo5c. Antibodies to Exo70 (R) do partially colocalize with GFP-Myo5c, particularly on the Myo5c tubules. The representative images in this figure are all single confocal planes.

and some puncta (Figure 4, P–R). This colocalization with a component of the exocyst complex (Yeaman *et al.*, 2004) suggests that the Myo5c-labeled tubules may function in an exocytic pathway.

Myo5c Localizes on Secretory Granules

Because EM studies have shown that MCF-7 cells contain secretory granules when cultured in the presence of the endogenous estrogens present in calf serum (Vic *et al.*, 1982), we tested if endogenous Myo5c associates with secretory granules. We therefore transfected MCF-7 cells with chromogranin A-GFP, a widely used marker protein that localizes to the lumen of secretory granules that undergo regulated secretion (Taupenot *et al.*, 2002). Although chromogranins were originally characterized in endocrine cells, they have also been detected in some exocrine cells (Kanno *et al.*, 1999; Hofsli *et al.*, 2002; Romeo *et al.*, 2002), and they are packaged within exocrine granules when expressed in exocrine cells (Natori *et al.*, 1998; Hofsli *et al.*, 2002). Confocal images revealed that chromogranin A-GFP localizes to discrete granules that exhibit striking colocalization with puncta of endogenous Myo5c (Figure 5, A–F). Although most Myo5c puncta colocalize with chromogranin A, some Myo5c puncta lack detectable chromogranin A labeling and some chromogranin A puncta lack detectable Myo5c labeling. Quantification of this data indicates that 67 ± 13% of Myo5c puncta (11 cells, 1180 puncta) are labeled by chromogranin A. Conversely, 69 ± 11% of chromogranin A granules (1201 puncta from 11 cells) were labeled by Myo5c. Interestingly, the Myo5c puncta with a ring-like appearance often surrounded individual chromogranin A granules (Figure 5, D–G). This relationship can also be seen in the linescan of an individual granule shown in Figure 5G. Because Myo5c is a cytoplasmic motor protein and chromogranin A is a lumenal marker for granules that undergo regulated secretion, these results strongly suggest that Myo5c associates with the cytoplasmic surface of secretory granules.

To confirm that Myo5c associates with secretory granules, we also tested whether exogenously expressed Myo5c localizes on secretory granules. MCF-7 cells were therefore cotransfected with chromogranin A-GFP and mCherry-Myo5c. Like endogenous Myo5c, mCherry-Myo5c localized to small puncta that showed striking colocalization with chromogranin A (Figure 5, H–J). The puncta labeled by Myo5c and chromogranin A-GFP frequently colocalized with small granules detectable by DIC microscopy. The tight association between Myo5c and secretory granules was also demonstrated by live-cell imaging using two-color TIRF in conjunction with DIC. Movies from these experiments showed that mCherry-Myo5c and chromogranin A-GFP clearly colocalize on moving granules (see Movie 4), thus providing extremely strong evidence that Myo5c associates with secretory granules in living MCF-7 cells.

To test whether the association of Myo5c with secretory granules was specific or a general property of class V myosins, we cotransfected MCF-7 cells with chromogranin A-GFP and a mCherry-Myo5b construct. Time-lapse imaging of these cells demonstrated that Myo5b exhibits little or no colocalization with chromogranin A–labeled secretory granules (Movie 5), consistent with our previous data showing little overlap between Myo5b and Myo5c.

We also tested whether Myo5c colocalized with a second marker for secretory granules, (Lang *et al.*, 1997; Desnos *et al.*, 2003, 2007b). Fluorescently tagged NPY consists of the signal sequence and part of the propeptide from NPY fused to either GFP or mRFP. Because NPY-GFP is a small and relatively soluble marker that is packaged into secretion granules, it has been widely used as a nonperturbing probe to allow direct visualization of secretory granule exocytosis (Lang *et al.*, 1997; El Meskini *et al.*, 2001; Desnos *et al.*, 2007b). We thus imaged MCF-7 cells cotransfected with NPY-GFP and mCherry-

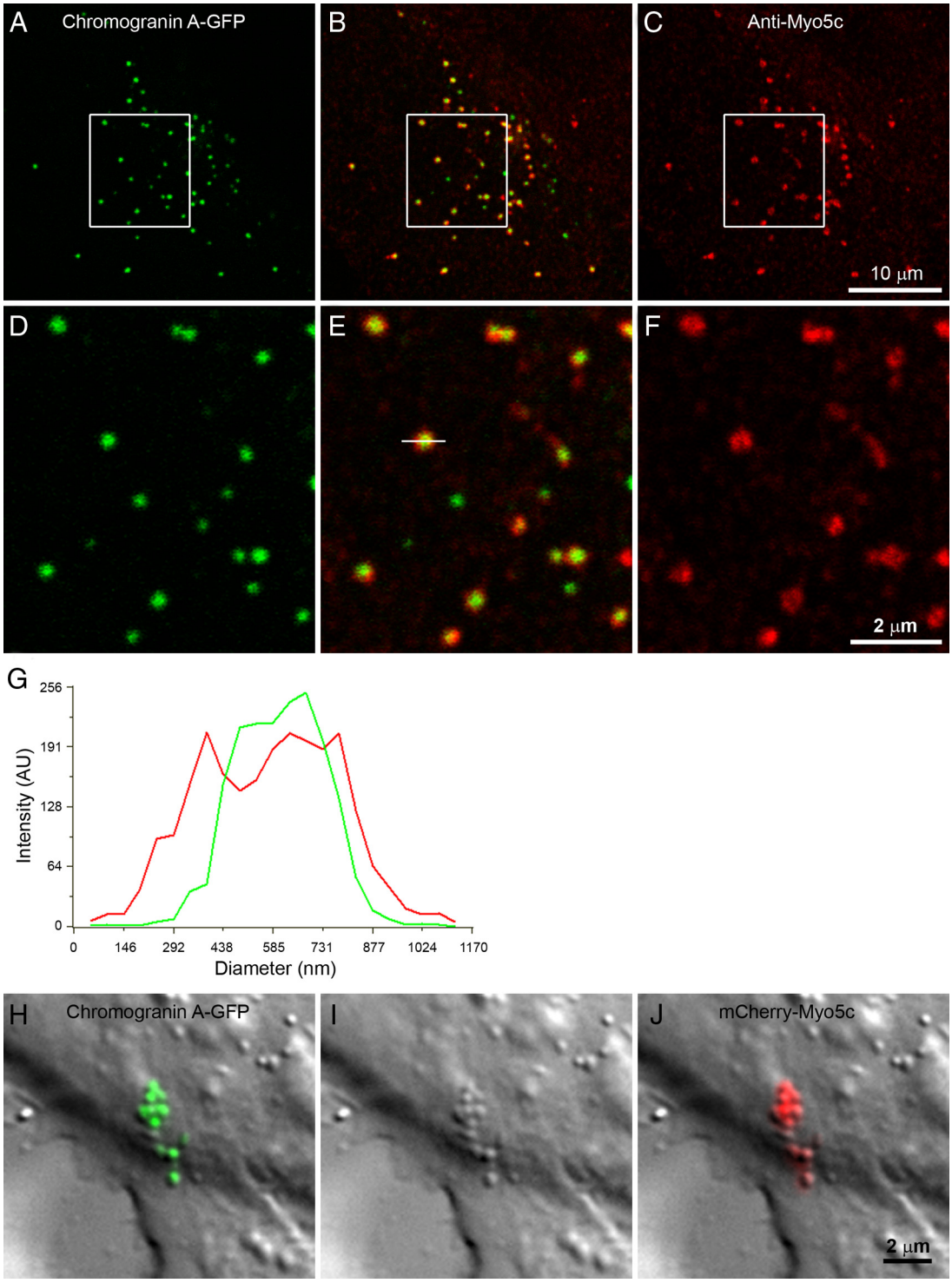

Figure 5. Myo5c localizes on secretory granules. (A–F) Endogenous Myo5c localizes on secretory granules labeled by chromogranin A-GFP. MCF-7 cells transfected with the secretory granule marker chromogranin A-GFP (green) were immunolabeled with anti-Myo5c antibodies (red). (D–F) Higher magnification views of the boxed region of the single confocal plane seen in A–C showing that a single Myo5c punctum often constitutes a ring-like structure surrounding a chromogranin A-GFP–labeled secretory granule. (G) Linescan analysis of a representative chromogranin A-GFP/Myo5c punctum (indicated by the white line left of center in E) showing Myo5c staining surrounding a chromogranin A-GFP–labeled granule. (H–J) Exogenously expressed mCherry-Myo5c also localizes on secretory granules labeled by chromogranin A-GFP. MCF-7 cells were cotransfected with chromogranin A-GFP (green) and mCherry-Myo5c (red) for ~1.5 d and then imaged by wide-field fluorescence (H and J) and DIC microscopy (I). See also Movie 4.

Myo5c. As expected, many of the Myo5c puncta showed clear colocalization with NPY-GFP (see Movie 6). Although both NPY and chromogranin A clearly labeled Myo5c puncta, we did not detect either granule marker on Myo5c tubules.

Myo5c-associated Granules Can Be Triggered to Undergo Secretion

Given the clear association of Myo5c with two different secretory granule markers, we asked if the granules labeled by Myo5c in MCF-7 cells were functionally capable of undergoing secretion. We thus cotransfected MCF-7 cells with mCherry Myo5c and NPY-GFP and then performed live-cell imaging with two-color TIRF and DIC. To stimulate secretion, we added ionomycin, an ionophore that leads to increased intracellular Ca^{2+} and that has been previously used to trigger secretion in MCF-7 cells (Flezar and Heisler, 1993; Vadlamudi *et al.*, 2000). Although we did not detect exocytotic events before addition of ionomycin, addition of 5 μM ionomycin triggered a series of exocytotic events over several minutes that could be recognized by the sudden loss of an individual granule's NPY-GFP fluorescence (see Movie 6). Careful inspection revealed that at the same time the NPY fluorescence was lost from a given granule, a dimple-like structure detectable in DIC often appeared on the membrane. This simultaneous visualization of secretion events by DIC and by loss of NPY fluorescence provides strong evidence that ionomycin induced the secretory granules to undergo exocytosis. Interestingly, although the NPY fluorescence associated with a given granule's exocytosis typically disappeared within the space of 3–6 s, the Myo5c fluorescence often remained detectable for an additional 10–60 s.

To provide additional evidence that Myo5c-associated granules are capable of undergoing exocytosis, we performed similar secretion experiments by transfecting cells that stably express GFP-Myo5c with NPY-mRFP (Figure 6 and Movie 7). The cell illustrated in this movie had relatively large granules (~1-μm diameter) and clearly demonstrates that individual granules are surrounded by a ring of Myo5c. Although ionomycin triggered the exocytosis of relatively few granules in this cell, several clear examples of granule secretion can be observed (Figure 6, A–C). In this sequence several granules moved into the TIRF field after ionomycin and eventually underwent exocytosis. It is also important to note that the number and dynamics of Myo5c puncta appeared very similar in cells whether or not they expressed NPY-mRFP (see Movie 8). Furthermore, adding ionomycin triggered apparent fusion events of Myo5c puncta both in cells that expressed NPY-mRFP and in cells that did not. Together these experiments demonstrate that 1) Myo5c associates with secretory granules in MCF-7 cells, 2) Myo5c-associated granules can be triggered to undergo exocytosis, and 3) Myo5c can remain associated with the granule membrane for tens of seconds after fusion.

Although the colocalization between Myo5c puncta and the NPY-mRFP secretory granule marker is striking, it is not perfect, and some NPY-labeled secretory granules lacked detectable Myo5c staining. The granules that lack Myo5c may represent immature secretory granules because at 5–10 h after transfection, the newly synthesized granule markers exhibited a diffuse staining pattern that showed little colocalization with Myo5c puncta (not shown). Because some Myo5c puncta lacked detectable labeling by secretory granule markers, Myo5c is likely to associate with as yet unidentified organelles in addition to secretory granules.

Dominant-Negative Myo5c Perturbs the Distribution of Secretory Granules

Given the clear association of both endogenous and exogenous Myo5c with secretory granules, we next used the Myo5c tail as a dominant negative to test whether Myo5c functions in secretory granule trafficking. The tail domains of class V myosins have been widely used as dominant negatives and yield phenotypes similar to those of genetic knockouts (Catlett and Weisman, 1998; Wu *et al.*, 1998; Reck-Peterson *et al.*, 1999; Schott *et al.*, 1999; Jones *et al.*, 2000). In the initial report on the discovery of Myo5c, we found that expressing the Myo5c tail in HeLa cells led to the formation of large puncta that specifically colocalized with and perturbed the distribution of Rab8a and transferrin receptor, but not the Golgi, late endosomes, lysosomes, or Rab11a-positive recycling endosomes (Rodriguez and Cheney, 2002). We thus transfected MCF-7 cells with a Myo5c full tail construct labeled with mCherry and tested if it perturbed the distribution of secretory granules labeled by chromogranin A-GFP. In control cells transfected with an empty mCherry vector, chromogranin A–labeled secretory granules exhibited their usual pattern of localization (Figure 7, A–C). In the cells transfected with the dominant negative mCherry-Myo5c full tail, however, chromogranin A localization was dramatically perturbed, and much of it formed large puncta or clumps that partially colocalized with the Myo5c tail (Figure 7, D–F).

To confirm these results, we tested if expression of the Myo5c tail perturbed the distribution of a second secretory granule marker, NPY-GFP. As shown in Figure 7, G–L, expressing the Myo5c tail also perturbed the distribution of NPY-GFP and led to the formation of large puncta that partially colocalized with the Myo5c tail. To quantify the effects of the Myo5c tail on the distribution of secretory granule markers, we calculated the fraction of total granule fluorescence per cell that was present in granules with apparent diameters greater than 1 μm. Because relatively little fluorescence in control cells is contributed by granules whose apparent diameters are greater than 1 μm, this provides a relatively simple assay of the effects of the Myo5c tail on secretory granule distribution. For cells expressing chromogranin A-GFP, this value more than doubled from 29 $\pm$ 11% in control cells to 70 $\pm$ 11% ($p < 0.01$) in cells transfected with the Myo5c tail (Figure 7M). Similar results were obtained for cells expressing NPY-mRFP as the granule marker (Figure 7N).

We also switched fluorescent tags and performed similar experiments to test if the GFP-Myo5c tail perturbed the distribution of secretory granules labeled with NPY-mRFP (Supplemental Figure S3). As observed above with the mCherry tag, expressing GFP-Myo5c full tail induced the formation of large NPY puncta that partially colocalized with the Myo5c tail. These effects appear to be specific to the GFP-Myo5c full tail construct because transfection with equivalent full tail constructs from Myo5a (GFP-Myo5a full tail) or Myo5b (GFP-Myo5b full tail) did not obviously perturb the distribution of the NPY-mRFP granule marker and showed little colocalization with it. Together these experiments indicate that the Myo5c tail domain is sufficient for targeting to secretory granules in MCF-7 cells and that dominant negative Myo5c perturbs the distribution of secretory granule markers.

Myo5c Puncta Are Labeled by Rab27b, and Myo5c Tubules Are Labeled by Rab8a

To confirm the results with exogenous granule markers, we next asked if Myo5c associated with endogenous markers of secretory granules. We therefore screened MCF-7 cells stably expressing GFP-Myo5c with a panel of antibodies to identify endogenous Rab proteins present on the two Myo5c compartments identified here (Figure 8). Myo5c puncta showed striking colocalization with Rab27b, a Rab protein that labels

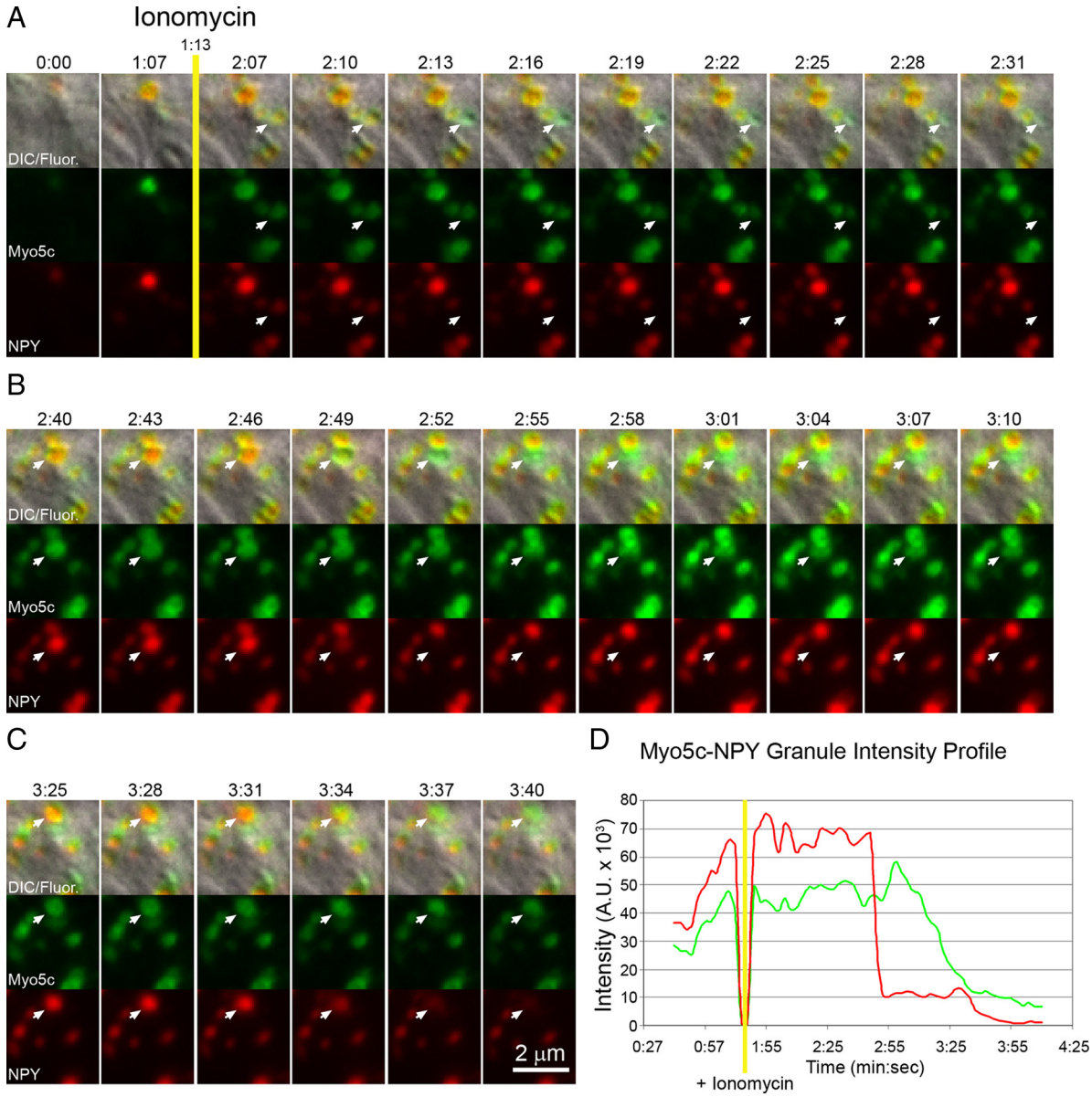

Figure 6. Myo5c-labeled secretory granules can be triggered to undergo secretion. MCF-7 cells stably expressing GFP-Myo5c were transiently transfected with NPY-mRFP to label secretory granules and stimulated to secrete with ionomycin (5 μM). (A–C) Image sequences from a movie showing several secretory events (arrows). Top, middle, and bottom panels of each sequence correspond to DIC-fluorescence overlay, GFP-Myo5c, and NPY-mRFP, respectively. (D) Fluorescence intensity profile of secretory event in B, showing Myo5c fluorescence remaining at site of secretion after granule contents were secreted. A circular region with a 1-μm diameter was used to track individual granules to obtain integrated intensity values. In A–C, the DIC images (top panels) show the formation of granule "dimples" during secretory events. Bottom panels, fluorescence image sequences were acquired using TIRF illumination. Note the appearance of many secretory granules into the TIRF field after ionomycin treatment. See Movie 7 to view the entire cell analyzed here.

secretory granules and functions as a "secretory Rab" (Chen *et al.*, 2004; Imai *et al.*, 2004; Fukuda, 2008). Myo5c puncta clearly colocalized with individual granules labeled by Rab27b (Figure 8, A–C, and inset), with 81 ± 8% of Myo5c puncta (1072 puncta from 12 cells) colocalizing with Rab27b. We next tested if Myo5c colocalized with Rab3d, another Rab protein that localizes on secretory granules (Valentijn *et al.*, 1996; Fukuda, 2008). Consistent with the results we reported in Marchelletta *et al.* (2008), Myo5c also colocalized with Rab3d (Figure 8, E and F). Although the Rab3d antibody yielded a relatively weak signal, 60 ± 16% of Myo5c puncta colocalized with Rab3d (882 puncta from 15 cells). Interestingly, we did not detect labeling of Myo5c tubules with either Rab27b or Rab3d. We therefore stained cells with antibodies to Rab8a, a Rab protein that accumulates with the Myo5c tail (Rodriguez and Cheney, 2002). This revealed that Myo5c tubules are labeled by Rab8a (Figure 8, G–I). However, Rab8a showed relatively little labeling of Myo5c puncta, and colocalization analysis indicated that only 21 ± 9% of Myo5c puncta overlapped with Rab8a fluorescence (1469 puncta from 15 cells). This is only slightly higher than the control colocalization of 7.6 ± 1.5% obtained in cells stained with nonimmune IgG (889 puncta from 14 cells). As an additional control, we also stained cells with Rab11a, a

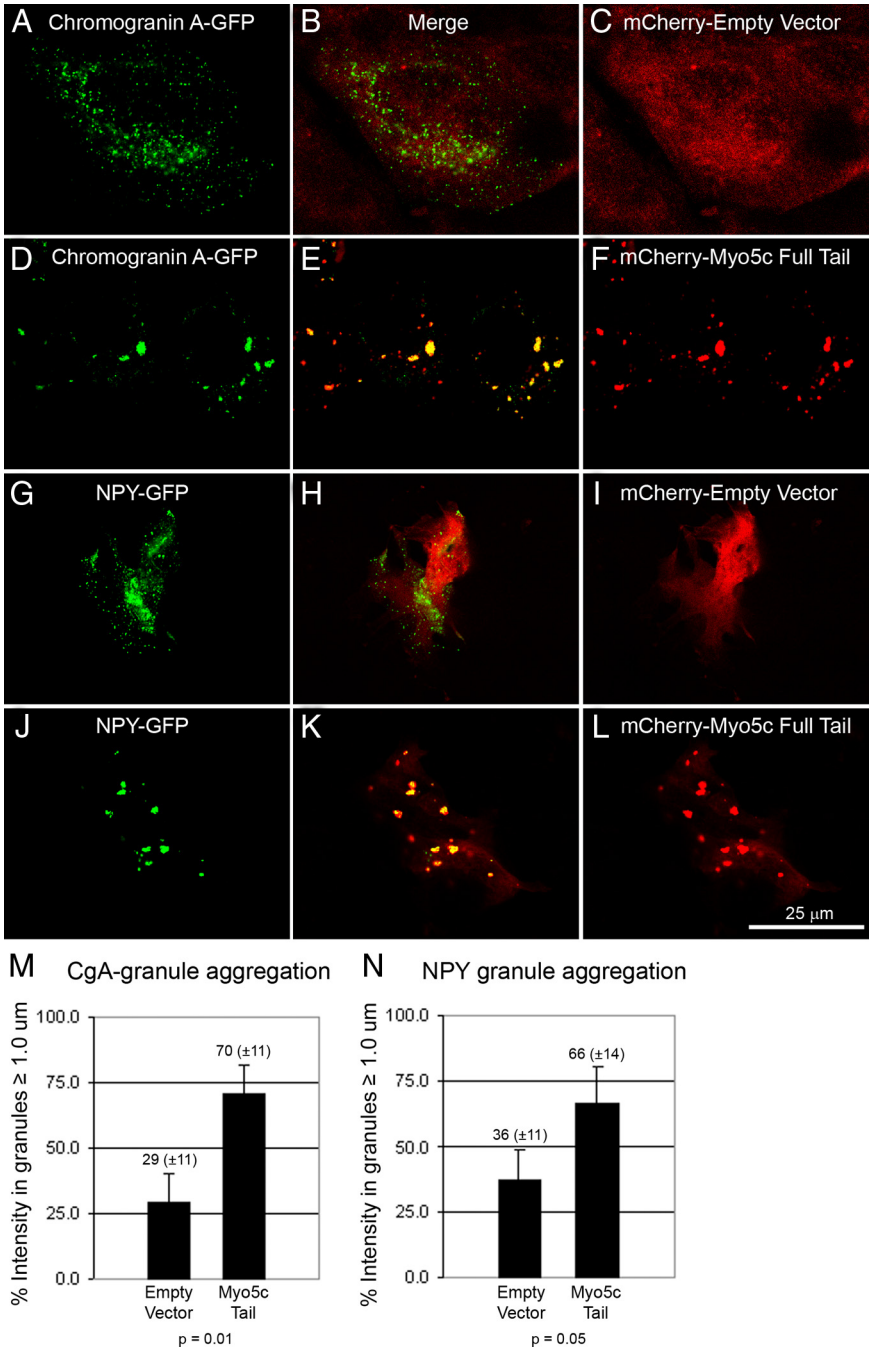

Figure 7. Dominant negative Myo5c disrupts the distribution of secretory granules. (A–F) MCF-7 cells were transfected for ~24 h with chromogranin A-GFP and either mCherry-empty vector (A–C) or mCherry-Myo5c full tail (D–F) and then imaged to analyze the distribution of secretory granules. Dominant negative Myo5c induced an obvious aggregation of the secretory granule marker into large puncta or clumps (D and E). (G–L) MCF-7 cells were transfected for ~36 h with NPY-GFP and either mCherry empty vector (G–I) or mCherry-Myo5c full tail (J–L) and then imaged to analyze the distribution of secretory granules. Dominant negative Myo5c also induced an obvious aggregation of this secretory granule marker into large puncta or clumps. Images are single confocal planes. (M and N) Bar graphs quantifying the effect of dominant negative Myo5c on secretory granule distribution. To quantify secretory granule aggregation, the percentage of total granule marker fluorescence per cell that was present in granules with effective diameters greater than 1 μm was calculated (see *Materials and Methods*; n = 3 experiments).

Rab protein that binds to Myo5b and labels the recycling endosome (Lapierre *et al.*, 2001). As expected, there was relatively little colocalization between Myo5c and Rab11a, with only 18.4 ± 6% of Myo5c puncta scored as overlapping with Rab11a fluorescence (717 puncta from 25 cells).

To further investigate the interaction between Myo5c and secretory granules, we generated a Myo5c construct that lacks the globular tail domain (GFP-Myo5c HMM) and tested if it associated with secretory granules labeled by endogenous Rab27b. Comparison with full-length GFP-Myo5c shows that deletion of the globular tail leads to a clear loss of colocalization with Rab27b (Supplemental Figure S4, A–F), thus demonstrating that the Myo5c globular tail is necessary for targeting to secretory granules. The construct lacking the globular tail also failed to perturb the distribution of Rab27b-labeled granules. The GFP-Myo5c full tail, on the other hand, induced the formation of large clumps of Rab27b. Because the association of Myo5a with melanosomes has been reported to be blocked by phosphorylation of a conserved serine present in the globular tails of all three class V myosins in mammals (Karcher *et al.*, 2001), we also generated a Myo5c tail construct containing a point mutation (S1539D) corresponding to the S1650D point mutation that inhibited the binding of Myo5a to melanosomes. Because the S1539D point mutant colocalized with Rab27b and induced the formation of large clumps of Rab27b, it is unlikely that phosphorylation at this site regulates the targeting of Myo5c to secretory granules in the same manner

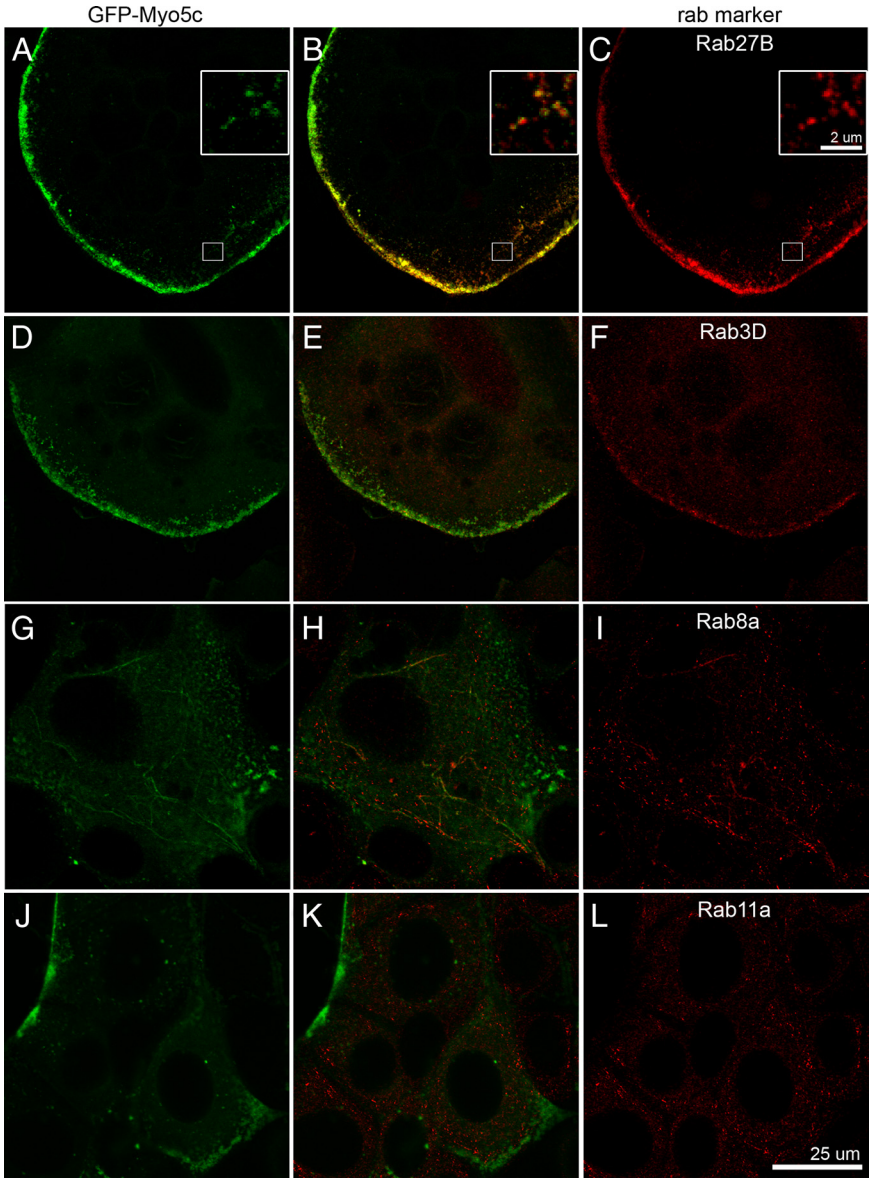

Figure 8. Identification of endogenous Rab proteins present on Myo5c puncta or tubules. MCF-7 cells that stably express GFP-Myo5c were stained with antibodies to the indicated Rab proteins. (A–C) Rab27b, an endogenous marker of secretory granules, exhibits striking colocalization with Myo5c puncta. Inset, a high-magnification view showing colocalization on individual granules. (D–F) Rab3d, another endogenous marker of secretory granules, also colocalizes with Myo5c puncta. (G–I) Rab8a colocalizes with Myo5c tubules, but exhibits relatively little labeling of Myo5c puncta. (J–L) Rab11a, a marker for the recycling endosome that binds to Myo5b, exhibits little colocalization with Myo5c on either puncta or tubules. Images are single confocal planes.

that phosphorylation of Myo5a regulates targeting to melanosomes.

How Many Myo5c Molecules Are Present per Secretory Granule?

Because Myo5c is reported to be nonprocessive (Watanabe *et al.*, 2007; Takagi *et al.*, 2008), we next sought to estimate the approximate number of Myo5c molecules present per secretory granule. We thus imaged MCF-7 cells stably expressing GFP-Myo5c using the same TIRF imaging conditions that we recently used to image the movements of GFP-Myo10 at the single-molecule level in living cells (Kerber *et al.*, 2009). We then measured the apparent diameters and integrated intensities of individual, well-resolved puncta of GFP-Myo5c (Supplemental Figure S5). To estimate the number of Myo5c molecules present per puncta, the integrated intensity of each puncta was divided by the average brightness of single GFP molecules imaged under these conditions (Kerber *et al.*, 2009) and corrected for the expression level data showing that ~56% of the Myo5c molecules in the stable cells are tagged with GFP. Using this method, Myo5c puncta with apparent diameters of 500–600 nm are calculated to have an average of 72 ± 39 Myo5c heavy chains. This corresponds to on the order of ~36 Myo5c dimers per granule. Although this calculation is likely to underestimate the actual number of Myo5c molecules present per granule because of factors such as the decreased intensity of the TIRF field with increased distance from the coverslip, it provides one of the first estimates of the number of myosin-V molecules present on an organelle in a living cell.

Does Myo5c Constantly Cycle On and Off Granule Membranes?

As a final approach to investigate the interaction between Myo5c and secretory granules, we took advantage of the high-resolution imaging made possible by the stable GFP-Myo5c cells to perform single granule FRAP (fluorescence recovery after photobleaching) experiments to characterize the exchange dynamics between Myo5c and its granule binding sites. GFP-Myo5c cells were transfected with NPY-mRFP

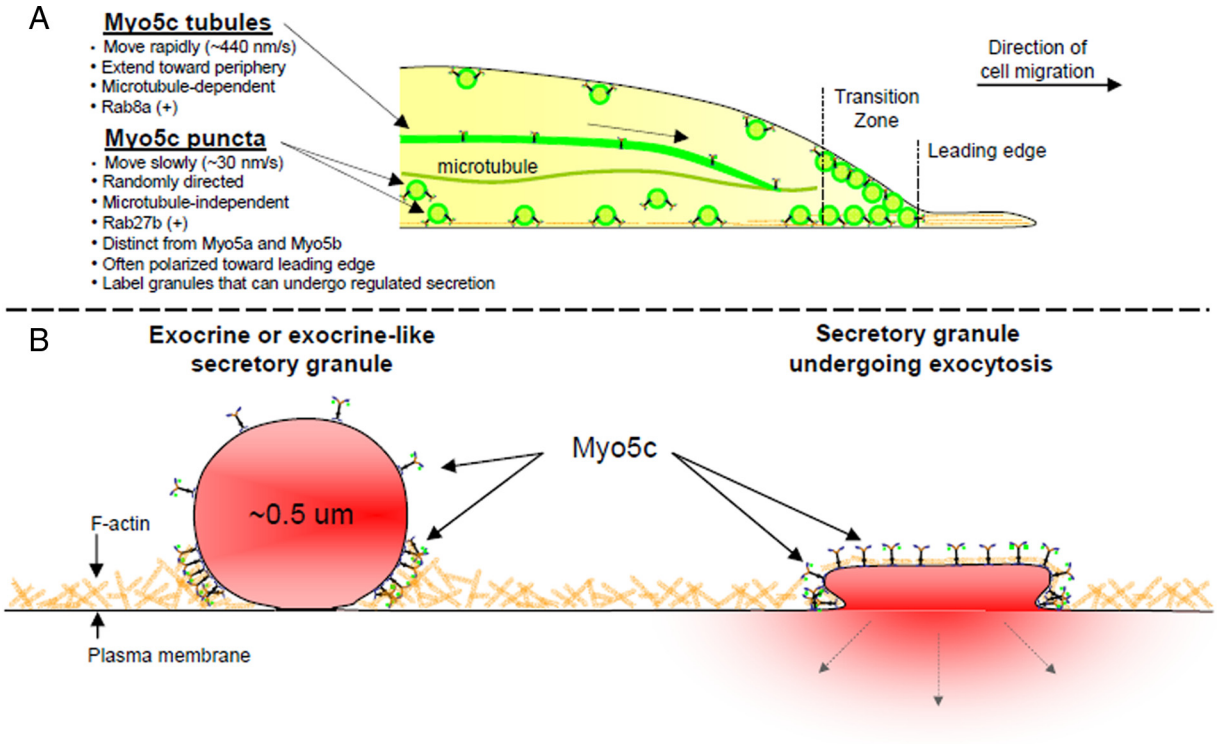

Figure 9. Diagram summarizing the localization and dynamics of Myo5c. (A) Schematic of an MCF-7 cell showing Myo5c associates with two distinct compartments that differ in their morphology, dynamics, microtubule dependence, and labeling by Rab proteins. (B) Higher magnification diagram illustrating that Myo5c is present on exocrine or exocrine-like secretory granules in the actin-rich cortex before, during, and shortly after exocytosis.

to label granules and were then imaged by live-cell confocal microscopy. When individual GFP-Myo5c puncta were bleached, we observed a gradual recovery of fluorescence over the course of ~500 s (Supplemental Figure S6 and Movie 9), indicating that a large fraction of the Myo5c on a granule is constantly cycling on and off under resting conditions. As a control, we simultaneously bleached the NPY-mRFP granule marker, and as expected for a lumenal protein, it showed no recovery after photobleaching. Although the low level of fluorescence makes detailed analysis of the single granule FRAP curves difficult, to our knowledge these experiments represent the first time that the exchange dynamics of a class V myosin with its target organelle have been investigated in a living cell. The clear qualitative conclusion from these experiments is that half or more of the Myo5c molecules on a secretory granule exchange over a time course of several hundred seconds.

DISCUSSION

Although class V myosins play critical roles in organelle trafficking and have been the subject of intensive research, relatively little is known about Myo5c. Here we provide the first immunolocalization of endogenous Myo5c in a cell line and the first live-cell imaging of GFP-Myo5c. These experiments showed that Myo5c associates with at least two compartments: small puncta and slender tubules (Figure 9). We also show that the localization and dynamics of Myo5c are distinct from those of Myo5b. Most importantly, we show that Myo5c localizes on secretory granules and that dominant negative Myo5c dramatically perturbs the distribution of secretory granule markers. As discussed below, these results help define the fundamental cell biology of Myo5c and indicate that Myo5c functions as a molecular motor in the trafficking of exocrine secretory granules.

Myo5c Associates with Slender Tubules That Move Rapidly and Microtubule Dependently

The morphology, dynamics, and microtubule dependence of the Myo5c-associated tubules strongly suggest they correspond to membranous tubules. Membranous tubules have been implicated in many different trafficking pathways, including exocytic recycling pathways such as those utilized by the transferrin receptor (Hopkins *et al.*, 1994) or MHCI (major histocompatibility complex I; Weigert *et al.*, 2004). Because Myo5c is an actin-dependent motor and the tubule movements that we observed were inhibited by nocodazole, the Myo5c on tubules is likely to be a passenger on membranous tubules that are undergoing rapid transport along microtubules. Although the precise identity and functions of the Myo5c tubules are not yet clear, they were labeled with Rab8a. There is precedent for an association between Myo5c and Rab8a because we previously showed that the GFP-Myo5c tail labeled slender tubules present in a subset of HeLa cells and that expression of the Myo5c tail induced the formation of large puncta labeled by Rab8a and transferrin receptor (Rodriguez and Cheney, 2002). Consistent with this, a recent study reported that Myo5c binds to Rab8a and that Rab8a localizes to slender tubules detected in ~10% of HeLa cells and functions as part of a tubular recycling system distinct from the Rab11a recycling endosome (Roland *et al.*, 2007). Rab8a is reported to function in post-Golgi secretory trafficking (Peranen *et al.*, 1996; Ang *et al.*, 2003; Sato *et al.*, 2007; Henry and Sheff, 2008) and has also been

implicated in secretory granule formation (Faust *et al.,* 2008). Importantly, Myo5c tubules were detected in only a subset of MCF-7 cells, even under live-cell imaging conditions. This suggests that Myo5c tubules are associated with trafficking events that are either transient or induced in only a subset of cells.

Myo5c Puncta Move Slowly and Microtubule Independently

Endogenous Myo5c and GFP-Myo5c both localized to numerous small puncta. Because many GFP-Myo5c puncta could be imaged by TIRF, these puncta must be located at the cell cortex, where Myo5c could potentially interact with cortical actin filaments. Individual puncta often remained within the ~200-nm depth of the TIRF field for hundreds or thousands of seconds and thus are relatively long-lived under resting conditions. Although the Myo5c puncta exhibited little movement in the Z-axis, they moved constantly in the X-Y plane in a slow (~30 nm/s) and apparently random manner. These slow movements in the plane of the membrane are presumably due either to some form of tethered diffusion or to Myo5c motor activity. Because the slow movements continued in the presence of nocodazole, they are not dependent on microtubules. The slow movements are also unlikely to be driven by actin-based rocketing because we did not detect comet tails on Myo5c puncta when cells were stained with phalloidin (not shown). As an actin-based motor that localizes to exocrine or exocrine-like secretory granules, Myo5c is a strong candidate to power granule movement, although it should be noted that the ~30 nm/s velocity of the puncta is at the lower end of the 24–160 nm/s range of in vitro motility velocities reported for Myo5c (Watanabe *et al.,* 2007; Takagi *et al.,* 2008).

Do the Different Class V Myosins Have Distinct or Overlapping Functions?

An important result from this work is the demonstration that the localization of Myo5c is distinct from that of Myo5a or Myo5b. This indicates that the different class V myosins have different functions in MCF-7 cells. An important difference between Myo5c and the other class V myosins in mammals is that Myo5c appears to be nonprocessive (Watanabe *et al.,* 2007; Takagi *et al.,* 2008). Although processivity in myosins was first discovered in Myo5a (Mehta *et al.,* 1999), it is now known that several other class V myosins, including Myo2p (Reck-Peterson *et al.,* 2001) and *Drosophila* myosin V (Toth *et al.,* 2005), are not processive. Although processivity would potentially allow a single myosin molecule to transport an organelle, nonprocessive motors can also transport organelles if enough motors are present. Because biochemical studies with baculovirus expressed Myo5c constructs indicate a duty ratio of 0.10 (Takagi *et al.,* 2008) to 0.33 (Watanabe *et al.,* 2007), as few as 3–10 Myo5c molecules would be expected to be sufficient to transport an organelle processively. Because our measurements indicate that there are on the order of 36 Myo5c dimers per average granule, there is sufficient Myo5c per granule to power movement. Given the 36-nm step size of myosin V (Mehta *et al.,* 1999), however, it should be noted that very few steps would be required to span the entire depth of the TIRF field or actin-rich cortex.

Myo5c Associates with Secretory Granules and Functions in Secretory Granule Trafficking

Myo5c puncta exhibited striking colocalization with two different exogenous markers of secretory granules, chromogranin A-GFP, and fluorescently tagged NPY. Myo5c also colocalized with two different endogenous markers of secretory granules, Rab27b and Rab3d. The granules could also be triggered to undergo secretion, and the TIRF imaging of this provides the first live-cell imaging of the dynamics of Myo5c during exocytosis. This revealed that Myo5c often remains transiently associated with granule membranes for 10–60 s after exocytosis. To test if Myo5c functions in secretory granule trafficking, we expressed the dominant negative Myo5c tail and found that it induced the formation of large puncta that partially colocalized with secretory granule markers and dramatically perturbed their distribution. These effects appear to be specific to Myo5c because equivalent tail constructs from Myo5a and Myo5b did not grossly perturb the distribution of secretory granules and showed little colocalization with secretory granule markers. Together these experiments provide strong evidence that Myo5c associates with secretory granules and is required for normal secretory granule trafficking.

Myo5c and Exocrine Secretion

Although MCF-7 cells provide a model system that is ideal for high-resolution imaging and investigation of the basic cell biology of Myo5c, it is also important to consider the functions of Myo5c in exocrine secretory tissues. In recent collaborative studies, we showed that Myo5c localizes on mature exocrine secretory granules in rabbit lacrimal gland acinar cells (Marchelletta *et al.,* 2008). Most importantly, expression of the Myo5c tail partially inhibited carbachol stimulated secretion, indicating that Myo5c is required for normal secretion in actual exocrine secretory cells. The combination of the data from lacrimal gland acinar cells, the proteomics data identifying Myo5c as one of the proteins present in membranes from exocrine secretory granules (Chen *et al.,* 2006), and the imaging data presented here with MCF-7 cells provide extremely strong evidence that Myo5c is a class V myosin that functions in the trafficking of exocrine secretory granules.

A key goal for future research will thus be to identify the precise step or steps where Myo5c functions in secretory granule trafficking. A myosin on secretory granules could potentially act at several different steps in granule trafficking, including termination of microtubule-dependent transport at the cell cortex (Wu *et al.,* 1998), tethering of granules to cortical actin (Wu *et al.,* 1998; Desnos *et al.,* 2003, 2007a), transport and distribution of granules within the plane of the cortex (Desnos *et al.,* 2003; Rudolf *et al.,* 2003; Varadi *et al.,* 2005), recruitment of granules to the cortex in response to signals for secretion (Nascimento *et al.,* 2003), transport of granules through the actin cortex to the plasma membrane during secretion (Valentijn *et al.,* 2000; Desnos *et al.,* 2007b), contraction of the granule membrane to facilitate expulsion of granule contents (Valentijn *et al.,* 1999; Jerdeva *et al.,* 2005; Yu and Bement, 2007), and recycling of granule membranes after exocytosis (Valentijn *et al.,* 1999; Bement *et al.,* 2000; Thorn *et al.,* 2004; Sokac *et al.,* 2006; Larina *et al.,* 2007). Importantly, there are now several reports demonstrating that Myo5a localizes to endocrine secretory granules and that perturbing Myo5a function perturbs endocrine granule distribution (for recent reviews see Eichler *et al.,* 2006; Desnos *et al.,* 2007a). The functions of Myo5c on exocrine granules may thus be similar to the functions of Myo5a on endocrine granules. This being said, there are a number of major differences between endocrine and exocrine secretion. Exocrine secretion is polarized to the apical rather than the basolateral surface, exocrine granules are typically larger than endocrine granules, and exocrine secretion often occurs

with a relatively slow time course (Lang *et al.*, 1997; Steyer *et al.*, 1997; Oheim *et al.*, 1998; Thorn *et al.*, 2004; Thorn and Parker, 2005; Sokac and Bement, 2006). In addition, exocrine cells often exhibit compound exocytosis and exocrine granule membranes can persist as empty vesicles or "ghosts" for tens to hundreds of seconds after fusion (Thorn and Parker, 2005).

It will also be important to determine how Myo5c is attached to secretory granules. We show here that the globular tail is necessary and sufficient for targeting to granules, and that mutation of a conserved serine in the tail does not appear to affect targeting. An obvious question for the future is whether the Myo5c tail is linked to exocrine granules via a specific docking complex analogous to the Rab27a-melanophilin complex that links the Myo5a tail to melanosomes (Wu *et al.*, 2002). Finally, because we show that Myo5c associates with both secretory granules and membrane tubules, it will also be important to determine the functions of Myo5c on the tubules and other compartments that this motor associates with.

ACKNOWLEDGMENTS

The authors thank Marvin Lai for assistance in generating GFP-Myo5c globular tail, Chi W. Pak for assistance with image analysis, and Drs. Sarah Hamm-Alvarez and Ron Marchelletta (University of Southern California) for helpful comments and suggestions. We also acknowledge the University of North Carolina (UNC) Neuroscience Center Confocal and Multi-Photon Imaging Facility for confocal imaging, the assistance of Kirk McNaughton of the UNC Cell and Molecular Physiology Histology Facility, and the University of Kansas Microscopy and Analytical Imaging Facility. D.T.J. was supported by a Porter Fellowship from the American Physiological Society and a UNC Sequoyah Dissertation Completion Fellowship. This research was supported by National Institutes of Health, National Institute on Deafness and Other Communicative Disorders Grant DC03299 to R.E.C.

REFERENCES

Ang, A. L., Folsch, H., Koivisto, U. M., Pypaert, M., and Mellman, I. (2003). The Rab8 GTPase selectively regulates AP-1B-dependent basolateral transport in polarized Madin-Darby canine kidney cells. J. Cell Biol. *163*, 339–350.

Belyantseva, I. A., Boger, E. T., Naz, S., Frolenkov, G. I., Sellers, J. R., Ahmed, Z. M., Griffith, A. J., and Friedman, T. B. (2005). Myosin-XVa is required for tip localization of whirlin and differential elongation of hair-cell stereocilia. Nat. Cell Biol. *7*, 148–156.

Bement, W. M., Benink, H., Mandato, C. A., and Swelstad, B. B. (2000). Evidence for direct membrane retrieval following cortical granule exocytosis in *Xenopus* oocytes and eggs. J. Exp. Zool. *286*, 767–775.

Berg, J. S., and Cheney, R. E. (2002). Myosin-X is an unconventional myosin that undergoes intrafilopodial motility. Nat. Cell Biol. *4*, 246–250.

Berg, J. S., Powell, B. C., and Cheney, R. E. (2001). A millennial myosin census. Mol. Biol. Cell *12*, 780–794.

Bergmann, J. E., Kupfer, A., and Singer, S. J. (1983). Membrane insertion at the leading edge of motile fibroblasts. Proc. Natl. Acad. Sci. USA *80*, 1367–1371.

Catlett, N. L., and Weisman, L. S. (1998). The terminal tail region of a yeast myosin-V mediates its attachment to vacuole membranes and sites of polarized growth. Proc. Natl. Acad. Sci. USA *95*, 14799–14804.

Chen, X., Li, C., Izumi, T., Ernst, S. A., Andrews, P. C., and Williams, J. A. (2004). Rab27b localizes to zymogen granules and regulates pancreatic acinar exocytosis. Biochem. Biophys. Res. Commun. *323*, 1157–1162.

Chen, X., Walker, A. K., Strahler, J. R., Simon, E. S., Tomanicek-Volk, S. L., Nelson, B. B., Hurley, M. C., Ernst, S. A., Williams, J. A., and Andrews, P. C. (2006). Organellar proteomics: analysis of pancreatic zymogen granule membranes. Mol. Cell Proteom. *5*, 306–312.

Cheney, R. E., O'Shea, M. K., Heuser, J. E., Coelho, M. V., Wolenski, J. S., Espreafico, E. M., Forscher, P., Larson, R. E., and Mooseker, M. S. (1993). Brain myosin-V is a two-headed unconventional myosin with motor activity. Cell *75*, 13–23.

Desnos, C., Huet, S., and Darchen, F. (2007a). 'Should I stay or should I go?': myosin V function in organelle trafficking. Biol. Cell *99*, 411–423.

Desnos, C., Huet, S., Fanget, I., Chapuis, C., Bottiger, C., Racine, V., Sibarita, J. B., Henry, J. P., and Darchen, F. (2007b). Myosin va mediates docking of secretory granules at the plasma membrane. J. Neurosci. *27*, 10636–10645.

Desnos, C., *et al.* (2003). Rab27A and its effector MyRIP link secretory granules to F-actin and control their motion towards release sites. J. Cell Biol. *163*, 559–570.

Eichler, T. W., Kogel, T., Bukoreshtliev, N. V., and Gerdes, H. H. (2006). The role of myosin Va in secretory granule trafficking and exocytosis. Biochem. Soc. Trans. *34*, 671–674.

El Meskini, R., Jin, L., Marx, R., Bruzzaniti, A., Lee, J., Emeson, R., and Mains, R. (2001). A signal sequence is sufficient for green fluorescent protein to be routed to regulated secretory granules. Endocrinology *142*, 864–873.

Espreafico, E. M., Cheney, R. E., Matteoli, M., Nascimento, A. A., De Camilli, P. V., Larson, R. E., and Mooseker, M. S. (1992). Primary structure and cellular localization of chicken brain myosin-V (p190), an unconventional myosin with calmodulin light chains. J. Cell Biol. *119*, 1541–1557.

Evans, C. M., *et al.* (2004). Mucin is produced by clara cells in the proximal airways of antigen-challenged mice. Am. J. Respir. Cell Mol. Biol. *31*, 382–394.

Fan, G. H., Lapierre, L. A., Goldenring, J. R., Sai, J., and Richmond, A. (2004). Rab11-family interacting protein 2 and myosin Vb are required for CXCR2 recycling and receptor-mediated chemotaxis. Mol. Biol. Cell *15*, 2456–2469.

Faust, F., Gomez-Lazaro, M., Borta, H., Agricola, B., and Schrader, M. (2008). Rab8 is involved in zymogen granule formation in pancreatic acinar AR42J cells. Traffic *9*, 964–979.

Flezar, M., and Heisler, S. (1993). P2-purinergic receptors in human breast tumor cells: coupling of intracellular calcium signaling to anion secretion. J. Pharmacol. Exp. Ther. *265*, 1499–1510.

Fukuda, M. (2008). Regulation of secretory vesicle traffic by Rab small GTPases. Cell Mol. Life Sci. *65*, 2801–2813.

Henry, L., and Sheff, D. R. (2008). Rab8 regulates basolateral secretory, but not recycling, traffic at the recycling endosome. Mol. Biol. Cell *19*, 2059–2068.

Hofsli, E., Thommesen, L., Norsett, K., Falkmer, S., Syversen, U., Sandvik, A., and Laegreid, A. (2002). Expression of chromogranin A and somatostatin receptors in pancreatic AR42J cells. Mol. Cell Endocrinol. *194*, 165–173.

Hopkins, C. R., Gibson, A., Shipman, M., Strickland, D. K., and Trowbridge, I. S. (1994). In migrating fibroblasts, recycling receptors are concentrated in narrow tubules in the pericentriolar area, and then routed to the plasma membrane of the leading lamella. J. Cell Biol. *125*, 1265–1274.

Imai, A., Yoshie, S., Nashida, T., Shimomura, H., and Fukuda, M. (2004). The small GTPase Rab27B regulates amylase release from rat parotid acinar cells. J. Cell Sci. *117*, 1945–1953.

Jerdeva, G. V., Wu, K., Yarber, F. A., Rhodes, C. J., Kalman, D., Schechter, J. E., and Hamm-Alvarez, S. F. (2005). Actin and non-muscle myosin II facilitate apical exocytosis of tear proteins in rabbit lacrimal acinar epithelial cells. J. Cell Sci. *118*, 4797–4812.

Johnston, G. C., Prendergast, J. A., and Singer, R. A. (1991). The *Saccharomyces cerevisiae* MYO2 gene encodes an essential myosin for vectorial transport of vesicles. J. Cell Biol. *113*, 539–551.

Jones, J. M., Huang, J. D., Mermall, V., Hamilton, B. A., Mooseker, M. S., Escayg, A., Copeland, N. G., Jenkins, N. A., and Meisler, M. H. (2000). The mouse neurological mutant flailer expresses a novel hybrid gene derived by exon shuffling between Gnb5 and Myo5a. Hum. Mol. Genet. *9*, 821–828.

Kanno, T., Asada, N., Yanase, H., Iwanaga, T., Ozaki, T., Nishikawa, Y., Iguchi, K., Mochizuki, T., Hoshino, M., and Yanaihara, N. (1999). Salivary secretion of highly concentrated chromogranin a in response to noradrenaline and acetylcholine in isolated and perfused rat submandibular glands. Exp. Physiol. *84*, 1073–1083.

Karcher, R. L., Roland, J. T., Zappacosta, F., Huddleston, M. J., Annan, R. S., Carr, S. A., and Gelfand, V. I. (2001). Cell cycle regulation of myosin-V by calcium/calmodulin-dependent protein kinase II. Science *293*, 1317–1320.

Karpova, T. S., Reck-Peterson, S. L., Elkind, N. B., Mooseker, M. S., Novick, P. J., and Cooper, J. A. (2000). Role of actin and Myo2p in polarized secretion and growth of *Saccharomyces cerevisiae*. Mol. Biol. Cell *11*, 1727–1737.

Kerber, M. L., Jacobs, D. T., Campagnola, L., Dunn, B. D., Yin, T., Sousa, A. D., Quintero, O. A., and Cheney, R. E. (2009). A novel form of motility in filopodia revealed by imaging myosin-X at the single-molecule level. Curr. Biol. *19*, 967–973.

Lang, T., Wacker, I., Steyer, J., Kaether, C., Wunderlich, I., Soldati, T., Gerdes, H. H., and Almers, W. (1997). Ca^{2+}-triggered peptide secretion in single cells imaged with green fluorescent protein and evanescent-wave microscopy. Neuron *18*, 857–863.

Langford, G. M. (2002). Myosin-V, a versatile motor for short-range vesicle transport. Traffic *3*, 859–865.

Lapierre, L. A., *et al.* (2001). Myosin vb is associated with plasma membrane recycling systems. Mol. Biol. Cell *12*, 1843–1857.

Larina, O., Bhat, P., Pickett, J. A., Launikonis, B. S., Shah, A., Kruger, W. A., Edwardson, J. M., and Thorn, P. (2007). Dynamic regulation of the large exocytotic fusion pore in pancreatic acinar cells. Mol. Biol. Cell *18*, 3502–3511.

Lise, M. F., *et al.* (2006). Involvement of myosin Vb in glutamate receptor trafficking. J. Biol. Chem. *281*, 3669–3678.

Marchelletta, R. R., Jacobs, D. T., Schechter, J. E., Cheney, R. E., and Hamm-Alvarez, S. F. (2008). The class V myosin motor, Myosin 5c, localizes to mature secretory vesicles and facilitates exocytosis in lacrimal acini. Am. J. Physiol. Cell Physiol. *295*, C13–C28.

Mehta, A. D., Rock, R. S., Rief, M., Spudich, J. A., Mooseker, M. S., and Cheney, R. E. (1999). Myosin-V is a processive actin-based motor. Nature *400*, 590–593.

Mercer, J. A., Seperack, P. K., Strobel, M. C., Copeland, N. G., and Jenkins, N. A. (1991). Novel myosin heavy chain encoded by murine dilute coat colour locus. Nature *349*, 709–713.

Moores, S. L., Sabry, J. H., and Spudich, J. A. (1996). Myosin dynamics in live *Dictyostelium* cells. Proc. Natl. Acad. Sci. USA *93*, 443–446.

Nascimento, A. A., Roland, J. T., and Gelfand, V. I. (2003). Pigment cells: a model for the study of organelle transport. Annu. Rev. Cell Dev. Biol. *19*, 469–491.

Natori, S., King, A., Hellwig, A., Weiss, U., Iguchi, H., Tsuchiya, B., Kameya, T., Takayanagi, R., Nawata, H., and Huttner, W. B. (1998). Chromogranin B (secretogranin I), a neuroendocrine-regulated secretory protein, is sorted to exocrine secretory granules in transgenic mice. EMBO J. *17*, 3277–3289.

Oheim, M., Loerke, D., Stuhmer, W., and Chow, R. H. (1998). The last few milliseconds in the life of a secretory granule. Docking, dynamics and fusion visualized by total internal reflection fluorescence microscopy (TIRFM). Eur. Biophys. J. *27*, 83–98.

Pashkova, N., Jin, Y., Ramaswamy, S., and Weisman, L. S. (2006). Structural basis for myosin V discrimination between distinct cargoes. EMBO J. *25*, 693–700.

Pastural, E., Barrat, F. J., Dufourcq-Lagelouse, R., Certain, S., Sanal, O., Jabado, N., Seger, R., Griscelli, C., Fischer, A., and de Saint Basile, G. (1997). Griscelli disease maps to chromosome 15q21 and is associated with mutations in the myosin-Va gene. Nat. Genet. *16*, 289–292.

Peranen, J., Auvinen, P., Virta, H., Wepf, R., and Simons, K. (1996). Rab8 promotes polarized membrane transport through reorganization of actin and microtubules in fibroblasts. J. Cell Biol. *135*, 153–167.

Provance, D. W., and Mercer, J. A. (1999). Myosin-V: head to tail. Cell Mol. Life Sci. *56*, 233–242.

Pruyne, D. W., Schott, D. H., and Bretscher, A. (1998). Tropomyosin-containing actin cables direct the Myo2p-dependent polarized delivery of secretory vesicles in budding yeast. J. Cell Biol. *143*, 1931–1945.

Reck-Peterson, S. L., Novick, P. J., and Mooseker, M. S. (1999). The tail of a yeast class V myosin, myo2p, functions as a localization domain. Mol. Biol. Cell *10*, 1001–1017.

Reck-Peterson, S. L., Tyska, M. J., Novick, P. J., and Mooseker, M. S. (2001). The yeast class V myosins, Myo2p and Myo4p, are nonprocessive actin-based motors. J. Cell Biol. *153*, 1121–1126.

Rodriguez, O. C., and Cheney, R. E. (2002). Human myosin-Vc is a novel class V myosin expressed in epithelial cells. J. Cell Sci. *115*, 991–1004.

Roland, J. T., Kenworthy, A. K., Peranen, J., Caplan, S., and Goldenring, J. R. (2007). Myosin Vb interacts with Rab8a on a tubular network containing EHD1 and EHD3. Mol. Biol. Cell *18*, 2828–2837.

Romeo, R., Pellitteri, R., Mazzone, V., and Marcello, M. F. (2002). Chromogranin A expression in human colonic adenocarcinoma. Ital. J. Anat. Embryol. *107*, 177–183.

Rose, S. D., Lejen, T., Casaletti, L., Larson, R. E., Pene, T. D., and Trifaro, J. M. (2002). Molecular motors involved in chromaffin cell secretion. Ann. NY Acad. Sci. *971*, 222–231.

Rudolf, R., Kogel, T., Kuznetsov, S. A., Salm, T., Schlicker, O., Hellwig, A., Hammer, J. A., 3rd, and Gerdes, H. H. (2003). Myosin Va facilitates the distribution of secretory granules in the F-actin rich cortex of PC12 cells. J. Cell Sci. *116*, 1339–1348.

Sato, T., *et al.* (2007). The Rab8 GTPase regulates apical protein localization in intestinal cells. Nature *448*, 366–369.

Schmoranzer, J., Kreitzer, G., and Simon, S. M. (2003). Migrating fibroblasts perform polarized, microtubule-dependent exocytosis towards the leading edge. J. Cell Sci. *116*, 4513–4519.

Schott, D., Ho, J., Pruyne, D., and Bretscher, A. (1999). The COOH-terminal domain of Myo2p, a yeast myosin V, has a direct role in secretory vesicle targeting. J. Cell Biol. *147*, 791–808.

Sokac, A. M., and Bement, W. M. (2006). Kiss-and-coat and compartment mixing: coupling exocytosis to signal generation and local actin assembly. Mol. Biol. Cell *17*, 1495–1502.

Sokac, A. M., Schietroma, C., Gundersen, C. B., and Bement, W. M. (2006). Myosin-1c couples assembling actin to membranes to drive compensatory endocytosis. Dev. Cell *11*, 629–640.

Steyer, J. A., Horstmann, H., and Almers, W. (1997). Transport, docking and exocytosis of single secretory granules in live chromaffin cells. Nature *388*, 474–478.

Swiatecka-Urban, A., *et al.* (2007). Myosin Vb is required for trafficking of the cystic fibrosis transmembrane conductance regulator in Rab11a-specific apical recycling endosomes in polarized human airway epithelial cells. J. Biol. Chem. *282*, 23725–23736.

Takagi, Y., Yang, Y., Fujiwara, I., Jacobs, D., Cheney, R. E., Sellers, J. R., and Kovacs, M. (2008). Human myosin Vc is a low duty ratio, non-processive molecular motor. J. Biol. Chem. *283*, 8527–8537.

Takagishi, Y., Oda, S., Hayasaka, S., Dekker-Ohno, K., Shikata, T., Inouye, M., and Yamamura, H. (1996). The dilute-lethal (dl) gene attacks a Ca^{2+} store in the dendritic spine of Purkinje cells in mice. Neurosci. Lett. *215*, 169–172.

Taupenot, L., Harper, K. L., Mahapatra, N. R., Parmer, R. J., Mahata, S. K., and O'Connor, D. T. (2002). Identification of a novel sorting determinant for the regulated pathway in the secretory protein chromogranin A. J. Cell Sci. *115*, 4827–4841.

Thorn, P., Fogarty, K. E., and Parker, I. (2004). Zymogen granule exocytosis is characterized by long fusion pore openings and preservation of vesicle lipid identity. Proc. Natl. Acad. Sci. USA *101*, 6774–6779.

Thorn, P., and Parker, I. (2005). Two phases of zymogen granule lifetime in mouse pancreas: ghost granules linger after exocytosis of contents. J. Physiol. *563*, 433–442.

Toth, J., Kovacs, M., Wang, F., Nyitray, L., and Sellers, J. R. (2005). Myosin V from Drosophila reveals diversity of motor mechanisms within the myosin V family. J. Biol. Chem. *280*, 30594–30603.

Trybus, K. M. (2008). Myosin V from head to tail. Cell Mol. Life Sci. *65*, 1378–1389.

Vadlamudi, R. K., Wang, R. A., Talukder, A. H., Adam, L., Johnson, R., and Kumar, R. (2000). Evidence of Rab3A expression, regulation of vesicle trafficking, and cellular secretion in response to heregulin in mammary epithelial cells. Mol. Cell. Biol. *20*, 9092–9101.

Valentijn, J. A., Sengupta, D., Gumkowski, F. D., Tang, L. H., Konieczko, E. M., and Jamieson, J. D. (1996). Rab3D localizes to secretory granules in rat pancreatic acinar cells. Eur. J. Cell Biol. *70*, 33–41.

Valentijn, J. A., Valentijn, K., Pastore, L. M., and Jamieson, J. D. (2000). Actin coating of secretory granules during regulated exocytosis correlates with the release of rab3D. Proc. Natl. Acad. Sci. USA *97*, 1091–1095.

Valentijn, K. M., Gumkowski, F. D., and Jamieson, J. D. (1999). The subapical actin cytoskeleton regulates secretion and membrane retrieval in pancreatic acinar cells. J. Cell Sci. *112*(Pt 1), 81–96.

Vallotton, P., and Small, J. V. (2009). Shifting views on the leading role of the lamellipodium in cell migration: speckle tracking revisited. J. Cell Sci. *122*, 1955–1958.

Varadi, A., Tsuboi, T., and Rutter, G. A. (2005). Myosin Va transports dense core secretory vesicles in pancreatic MIN6 beta-cells. Mol. Biol. Cell *16*, 2670–2680.

Vic, P., Vignon, F., Derocq, D., and Rochefort, H. (1982). Effect of estradiol on the ultrastructure of the MCF7 human breast cancer cells in culture. Cancer Res. *42*, 667–673.

Watanabe, S., Mabuchi, K., Ikebe, R., and Ikebe, M. (2006). Mechanoenzymatic characterization of human myosin Vb. Biochemistry *45*, 2729–2738.

Watanabe, S., Watanabe, T., Sato, O., Awata, J., Homma, K., Umeki, N., Higuchi, H., Ikebe, R., and Ikebe, M. (2007). Human myosin Vc is a low duty ratio non-processive motor. J. Biol. Chem. *283*, 10581–10592.

Weigert, R., Yeung, A. C., Li, J., and Donaldson, J. G. (2004). Rab22a regulates the recycling of membrane proteins internalized independently of clathrin. Mol. Biol. Cell *15*, 3758–3770.

Wu, X., Bowers, B., Rao, K., Wei, Q., and Hammer, J. A., 3rd. (1998). Visualization of melanosome dynamics within wild-type and dilute mela-

nocytes suggests a paradigm for myosin V function In vivo. J. Cell Biol. *143*, 1899–1918.

Wu, X., Sakamoto, T., Zhang, F., Sellers, J. R., and Hammer, J. A., 3rd. (2006). In vitro reconstitution of a transport complex containing Rab27a, melanophilin and myosin Va. FEBS Lett. *580*, 5863–5868.

Wu, X. S., Rao, K., Zhang, H., Wang, F., Sellers, J. R., Matesic, L. E., Copeland, N. G., Jenkins, N. A., and Hammer, J. A., 3rd. (2002). Identification of an organelle receptor for myosin-Va. Nat. Cell Biol. *4*, 271–278.

Yeaman, C., Grindstaff, K. K., and Nelson, W. J. (2004). Mechanism of recruiting Sec6/8 (exocyst) complex to the apical junctional complex during polarization of epithelial cells. J. Cell Sci. *117*, 559–570.

Yu, H. Y., and Bement, W. M. (2007). Multiple myosins are required to coordinate actin assembly with coat compression during compensatory endocytosis. Mol. Biol. Cell *18*, 4096–4105.

Yvon, A. M., and Wadsworth, P. (2000). Region-specific microtubule transport in motile cells. J. Cell Biol. *151*, 1003–1012.

Zhang, H., Berg, J. S., Li, Z., Wang, Y., Lang, P., Sousa, A. D., Bhaskar, A., Cheney, R. E., and Stromblad, S. (2004). Myosin-X provides a motor-based link between integrins and the cytoskeleton. Nat. Cell Biol. *6*, 523–531.

Zhao, L. P., Koslovsky, J. S., Reinhard, J., Bahler, M., Witt, A. E., Provance, D. W., Jr., and Mercer, J. A. (1996). Cloning and characterization of myr 6, an unconventional myosin of the dilute/myosin-V family. Proc. Natl. Acad. Sci. USA *93*, 10826–10831.